Journal of Biomedical Photonics & Engineering

by Samara National Research University

Volume 2, Issue 1 (March 2016)

Editorial Board

Editor-In-Chief

Valery V. Tuchin - Saratov National Research State University, Russian Federation; Institute of Precision Mechanics and Control RAS, Russian Federation

Deputy Editor-In-Chief

Valery P. Zakharov - Samara National Research University, Russian Federation

Editorial Board

Stefan Andersson-Engels (Lund University, Sweden), **Alexey N. Bashkatov** (Saratov State University, Russia), **Ekaterina Borisova** (Academician Emil Djakov Institute of Electronics, Bulgarian Academy of Sciences, Bulgaria), **Wei Chen** (University of Central Oklahoma, USA), **Arthur Chiou** (National Yang-Mind University, Taiwan), **Elina A. Genina** (Saratov State University, Russia), **Min Gu** (Swinburne University, Australia), **Nikolay G. Khlebtsov** (Institute of Biochemistry and Physiology of Plants and Microorganisms RAS, Russia), **Juergen Lademann** (Charite University Clinic, Germany), **Kirill V. Larin** (University of Houston, USA), **Martin Leahy** (University of Galway, Ireland), **Qingming Luo** (Huazhong University of Science and Technology, China), **Stephen J Matcher** (University of Sheffield, Great Britain), **Igor Meglinski** (University of Oulu, Finland), **Vladimir S. Pavelyev** (Image Processing Systems Institute RAS, Russia), **Francesco Pavone** (University of Florence, Italy), **Roberto Pini** (Institute of Applied Physics, Italy), **Igor A. Platonov** (Samara State Aerospace University, Russia), **Juergen Popp** (Institute of Photonic Technology, Germany), **Alexander V. Priezzhev** (Moscow State University, Russia), **David Sampson** (The University of Western Australia, Australia), **Alexander Savitsky** (Institute of Biochemistry RAS, Russia), **Alexander P. Shkurinov** (Moscow State University, Russia), **Peter So** (Massachusetts Institute of Technologies, USA), **Janis Spigulis** (University of Latvia, Latvia), **Ilya V.Turchin** (Institute of Applied Physics RAS, Russia), **Vladimir G. Volostnikov** (N.P.Lebedev Physical Institute, Russia), **Lihong V. Wang** (Washington University, USA), **Ruikang Wang** (University of Washington, USA), **Xunbin Wei** (Shanghai Jiao Tong University, China), **Dan Zhu** (Britton Chance Center for Biomedical Photonics, Huazhong University of Science and Technology, China).

Postal address:

39B Lukacheva st., room #301

Samara 443086, Russian Federation

© 2016 JBPE

Contents

Introduction

Special Issue: Laser and optical technologies in biomedicine and ecology 010101
Aleksandra M. Mayorova, Valeriy P. Zakharov

Regular papers

Mathematical model of laser radiation femtosecond interaction with human skin 010301
Pavel Rogov, Viktor Bespalov

The use of laser dynamical speckle interferometry in the study of cellular processes 010302
A. P. Vladimirov, I. A. Novoselova, Y. A. Mikhailova, A. A. Bakharev, D. I. Yakin

Ex vivo investigation of glycerol diffusion in skin tissue 010303
Vadim D. Genin, Daria K. Tuchina, Ali Jaafar Sadeq, Elina A. Genina, Valery V. Tuchin, Alexey N. Bashkatov

Diagnostics of liquid properties by the example of bioorganic solutions 010304
Alexander Malov, Anna Neupokoeva, Alexandra Sambyalova

Choosing the probe radiation wavelengths for noninvasive monitoring of haemoglobin in blood 010305
Igor L. Davydkin, Natalia S. Kozlova, Vadim N. Koniukhov, Tatiana P. Kuzmina, Elizaveta V. Mordvinova

Destruction of a spherical polystyrene microparticle in pulsed ultraviolet beam for micromanipulation purpose 010306
Roman V. Skidanov, Vadim S. Vasiliev

Craquelure structure of protein film modification under the laser radiation of different spectral range action 010307
Alexander N. Malov, Anna V. Neupokoeva, Evgeniya M. Kudryashova

 © 2016 JBPE

Special Issue: Laser and optical technologies in biomedicine and ecology

We are pleased to present the first issue of second volume of JBPE, which focuses on laser and optical technologies for study of biological tissues and biomedical applications. This Special Issue of the Journal of Biomedical Photonics & Engineering presents the selected papers of the Workshop "Biophotonics" of the XIII all-Russian Youth Samara conference-contest on optics and laser physics.

The XIII Youth Samara conference-contest on optics and laser physics was held in Samara Branch of P.N. Lebedev Physical Institute of Russian Academy of Sciences at November 11-14, 2015 with support of Russian Foundation for Basic Research (grant 15-32-10335), Administration of Samara Region and Samara SPIE Student Chapter. The conference program included lectures of leading scientists, reports of young PhDs and competition reports of students, graduate students and young researches on topical issues of coherent and quantum optics, contemporary problems of physical optics, spectroscopy and nanophotonics. The Workshop "Biophotonics" became one of the most numerous and popular seminar at the conference and included many interesting reports on applications of laser and optical techniques in biomedicine and ecology. It was held in Samara State Aerospace University (SSAU). The young scientists of SSAU Department of Laser and Biotechnical Systems annually take the most active part in the seminar. Optical methods for diagnostic of various etiology diseases as well as the optical express-techniques of implants monitoring are in the focus of their investigations. The studies were carried out with the use of backscattering spectroscopy, Raman spectroscopy, and optical coherent tomography.

Besides students and post-graduate students of SSAU, young researches from Moscow, Saint-Petersburg, Saratov, Ekaterinburg, Tomsk and Irkutsk participated in the seminar Biophotonics in 2015. Their studies covered a wide range of theoretical and applied issues from the development of theoretical models of interaction of laser radiation with tissue to express-algorithm design for monitoring bioorganic liquids or optimization of the systems intended on the solution of specific medical problems. The different processes in single cells, separate organs or tissues and the whole body as well as in model biological tissue have been studied. The results of these studies were presented in 14 oral reports and 10 poster presentation.

The contest of scientific reports was held in the framework of the conference and we are pleased to announce that the report of V. Genin was recognized as the best oral report at the workshop "Biophotonics". P. Rogov and I. Novoselova took the second and the third places correspondingly. The report of N. Kozlova became the best poster report on biomedical problems. This issue of JBPE will introduce you to selected papers of the participants of the workshop "Biophotonics" of the XIII All-Russian Youth Samara conference-contest on optics and laser physics, including the papers of aforementioned participants.

The paper of P. Rogov and V. Bespalov is focused on the creation of the mathematical model of impact of intensive femtosecond laser radiation onto the human skin. Due to wide spread of femtoseconds lasers and their use in biology and medicine the study seems to be very important. The authors properly notice the lack of standards for safe levels of energy of intense femtosecond laser radiation in Russian Federation. The proposed model may be useful for determination of the maximum acceptable energy levels in new standard.

The diffusion of glycerol solutions in the rat skin *ex vivo* is studied in the paper of V. Genin and co-authors. The relevance and practical useful of the research is determined by the fact that aqueous solutions of glycerol are biocompatible optical clearing agents used for the light scattering reduction and the transport of radiation to deeper tissue layers. The results obtained by the authors enable to evaluate the efficiency of glycerol aqueous solutions of various concentrations as the optical clearing agents for skin parameters control.

The research of A. Vladimirov, I. Novoselova and co-authors is focused on the development of the techniques of early diagnostics and complex treatment of various diseases based on the

methods of nondestructive control for physiological state of cells. The authors have used speckle-interferometric method allowing analyze the processes inside the cells. And the differences of processes inside and outside the cell as well as in its various parts can be found out with the use of the method.

The system of non-invasive monitoring of hemoglobin concentration with the use of pulse CO-oximetry technique is presented in the paper of I. Davydkin, N. Kozlova and co-authors. The authors' aim was to find out the optimal set of wavelengths of the probing radiation to minimize the inaccuracy for the determining the hemoglobin concentration. It was shown that while using only four semiconductor laser units (only 4 wavelengths) the obtained accuracy was comparable with accuracy which commercially available monitors achieve with 12 wavelengths. As a result such unit is acceptable for the screening-diagnostics of population in order to identify individuals with potential pathologies. Reduction of the number of probe units resulted in simplification of the scheme and its cost.

The Issue includes two papers of the researches from Irkutsk State Medical University: A. Malov and co-authors. The techniques of monitoring structural changes in bioorganic liquids under laser radiation impact are presented in the first one. The solution ‘grippferon’ with the base component interferon Alfa-2b as well as the gelatin solution are used as the impact objects. The authors have proposed quick software algorithms for processing speckle patterns and crystallograms, allowing the comparison of the images at different stages of the monitoring.

In their second paper A. Malov and co-authors demonstrated the results of the study of thin films of protein (albumin) under the influence of laser radiation. The so-called craquelure-structure – the structure of cracks generated on the albumin surface as the result of its drying – is formed. It was experimentally shown that the structure characteristics were changed under laser influence and depended on laser wavelength and energy density.

The study of R. Skidanov and V. Vasiliev is focused on the development of a contactless method of movement of microparticles by means of the explosion of polystyrene particles with focused laser radiation. The particles with the size more than 30 μm including biological ones can be moved with the use of proposed technique. The paper is focused on the modeling of heating of polystyrene particles.

Thus, the selected papers presented in this Special Issue, introduce you to the major current issues discussed at the workshop “Biophotonics” of the XIII All-Russian Youth Samara conference-contest on optics and laser physics.

Special issue Editors:

Aleksandra M. Mayorova, Samara Branch of P.N. Lebedev Physical Institute of Russian Academy of Sciences, Samara State Aerospace University

Valeriy P. Zakharov, Samara State Aerospace University

Mathematical model of laser radiation femtosecond interaction with human skin

Pavel Rogov*, and Viktor Bespalov
Saint-Petersburg National Research University of Information Technologies, Mechanics, and Optics, Kronverkskii Prospekt str. 49, Saint-Petersburg, 197101, Russia

* **e-mail:** RogovPU@niuitmo.ru

Abstract. We present a mathematical model of linear and nonlinear processes that occur under the action of femtosecond laser radiation on the cutaneous covering. The analysis is carried out and the analytical solution of the set of equations describing the dynamics of the electron and atomic subsystems is obtained. The results of the work can be used to determine the maximum acceptable energy, generated by femtosecond laser systems, and to develop Russian laser safety standards for femtosecond laser systems. © 2016 Journal of Biomedical Photonics & Engineering.

Keywords: laser safety, femtosecond radiation, self-focusing, skin.

Paper #2847 received 2015.12.30 revised manuscript received 2016.03.01; accepted for publication 2016.03.01; published online 2016.03.29. doi: 10.18287/JBPE16.02.010301

References

1. S. A. Akhmanov, V. A. Vysloukh, and A. S. Chirkin, Optics of femtosecond laser pulses, Moscow, Nauka (1988) [in Russian]. ISBN 5-02-013838-X.
2. C. Rulliere, Femtosecond laser pulses, Springer (2005). ISBN: 978-0-387-01769-3.
3. B. S. Yilbas, and A. F. M. Arif. "Laser short-pulse heating with time-varying intensity and thermal stress development in the lattice subsystem," Proceedings of the Institution of Mechanical Engineers, Part C: Journal of Mechanical Engineering Science 219(1), 73-81 (2005).
4. L. Habbema, R. Verhagen, R. Van Hal, Y. Liu, and B. Varghese, "Minimally invasive non-thermal laser technology using laser-induced optical breakdown for skin rejuvenation," Journal of Biophotonics 5(2), 194–199 (2011).
5. "GOST 50723-94: Laser Safety. General safety requirements for time-processing and operation of laser products," Moscow, Standards Publishing House (1995) [in Russian].
6. V. Sriramoju, and R. R. Alfano, "In vivo studies of ultrafast near-infrared laser tissue bonding and wound healing," Journal of Biomedical Optics 20(10), 108001 (2015).
7. A. E. Pushkareva, "Methods of mathematical modeling in tissue optics," SPb, ITMO, (2008) [in Russian].
8. I. Fredriksson, M. Larsson, and T. Strömberg, "Optical microcirculatory skin model: assessed by Monte Carlo simulations paired with in vivo laser Doppler flowmetry," Journal of Biomedical Optics 13(1), 014015 (2008).
9. P. Stampfli, and K. H. Bennemann, "Theory for the instability of the diamond structure of Si, Ge, and C induced by a dense electron-hole plasma," Physical Review B 42(11), 7163–7173 (1990).
10. P. Stampfli, and K. H. Bennemann, "Dynamical theory of the laser-induced lattice instability of silicon," Physical Review B 46(17), 10686–10692 (1992).
11. M. F. Kropman, "Dynamics of Water Molecules in Aqueous Solvation Shells," Science 291(5511), 2118–2120 (2001).
12. M. F. Kropman, H.-K. Nienhuys, and H. J. Bakker, "Real-Time Measurement of the Orientational Dynamics of Aqueous Solvation Shells in Bulk Liquid Water," Physical Review Letters 88(7), 077601 (2002).
13. V. P. Lipp, D. S. Ivanov, B. Rethfeld, and M. E. Garcia, "On the interatomic interaction potential that describes bond weakening in classical molecular-dynamic modelling," Journal of Optical Technology 81(5), 254–255 (2014).
14. R. V. Dyukin, G. A. Martsinovskiĭ, G. D. Shandybina, E. B. Yakovlev, I. D. Nikiforov, and I. V. Guk, "Dynamics of the permittivity of a semiconductor acted on by a femtosecond laser," Journal of Optical Technology 78(8), 558-562 (2011).

15. V. A. Serebryakov, E. V. Boiko, A. G. Kalintsev, A. F. Kornev, A. S. Narivonchik, and A. L. Pavlov "Laser mid-infrared spectral range for precision surgery," Opt J 82(12), 3-13 (2015).
16. I. V. Meglinski, and A. V. Doronin, "Monte Carlo modeling for the needs of biophotonics and biomedical optics," in Advanced Biophotonics: tissue optical sectioning, V. V. Tuchin, and R. K. Wang (eds.), Taylor & Francis (2012).
17. S. Jacques, and L. Wang, "Monte Carlo modelling of light transport in tissue," in Optical-thermal response of laser-irradiated tissue, A. J. Welch, M. J. C. van Gemert (eds.), Plenum Press, New York (1996).

1 Introduction

Femtosecond laser systems (FLSs) are widely used in science, technical applications and medical technologies [1, 2]. In spite of the fast development of femtosecond technologies and their application in biology and medicine, at present in the Russian Federation there are no standards of safe energy levels of high-intensity femtosecond laser radiation. Note that the mechanism of interaction of intense femtosecond laser radiation with matter essentially differs from that for the pulses of longer duration, since the interaction time is smaller than the time, necessary to excite the phonon subsystem [3]. Besides, the high power density that arises when using the FLSs leads to various nonlinear processes, such as self-focusing, two- and three-photon absorption, multiphoton and impact ionization, and for the high energy density to the optical breakdown. [4]. This process is of particular importance in the case of femtosecond radiation incident on biological tissues, since the high-intensity femtosecond radiation may be essentially dangerous for skin, vision, and other human organs [5].

In the present work, we consider the linear and nonlinear interaction of femtosecond laser radiation with skin and propose a mathematical model approximately describing particular interaction processes. In future, the model can be used to determine the maximal acceptable levels of FLS energy.

2 Interaction mechanism

2.1 Specific features of ultrashort-pulse lasers and the skin

The human skin is an optically turbid opaque medium (both the absorption and the scattering are present). At the same time, the skin is a heterogeneous structure containing the inclusions of different type and dimension (blood vessels, hair follicles, etc.), which essentially complicates the understanding of the processes that occur under the action of laser radiations on the cutaneous covering. The main elements of the skin are water (70%) and proteins (27%), and the main structure protein is collagen (nearly 70% of dry skin weight). The water molecules can be divided into two groups, the free ones and the ones included in protein compounds (bound state, e.g., the three-fold screw group of collagen binds nearly 500 water molecules [6]). Thus, in the first approximation the skin may be considered as water with protein inclusions close to dielectric materials in their electrodynamic properties.

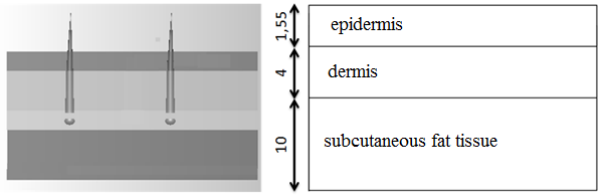


Fig. 1 Model of human skin.

Table 1 The mean optical (λ=800 nm) and thermal physical parameters used in the skin model for calculating [7].

Tissue	μa, 1/mm	μs, 1/mm	g	n	C, J/g·K	k, W/m·K	d, mm
Epidermis	0.083	21.37	0.85	1.5	3.05	0.29	0.03-2
Dermis	0.026	9.67	0.86	1.5	3.52	0.41	0.5-5
Subcutaneous fat	0.025	12.39	0.86	1.5	2.3	0.2	>10

Here μa is the absorption coefficient, μs is the scattering coefficient, g is the mean cosine of the scattering angle, n is the mean refractive index, C is the heat capacity, k is the heat conduction coefficient, d is the layer depth.

For estimate, we have chosen the wavelength 800 nm typical for the most widely used titanium-sapphire FLSs. The pulse duration in such systems can vary from 25 to 550 fs. The irradiation with ultrashort laser pulses leads to damages that cannot be explained by the thermal melting mechanism [8] and are due to the excitation of valence electrons by the laser pulses [9, 10]. The water molecules serve as the transmitting element that absorb the laser pulse energy and excite the vibrational (phonon) modes of collagen with the relaxation time of the order of 3 ps [11, 12].

2.2 Mathematical model

In the calculations, we used the set of balance equations that describe the dynamics of electron-atom subsystem. In the model the atoms interact via the semiempirical potentials and the electron degrees of freedom are not taken into account explicitly. The laser radiation generates non-equilibrium charge carriers described by the integral concentration [13]. In this case one can neglect the processes of Auger recombination and

impact ionization, since for the chosen parameters of radiation their semiempirical contribution is negligibly small.

E.B. Yakovlev et al. [11] proposed the idea of determining the dependence between the potentials of the atoms and the state of the electronic subsystem, thus making it possible to simulate the effects of heat transfer under the action of femtosecond pulses on dielectric materials. The differential Bouguer-Lambert law determines the distribution of the laser radiation intensity J(z,t) inside a solid. The system of heat transfer equation that describes the dynamics of electron and atom subsystems in the one-dimensional approximation has the form:

$$\frac{\partial T_e}{\partial t} = \alpha_e \frac{\partial^2 T_e}{\partial z^2} - \frac{1}{C_e \tau_{ep}}(T_e - T_a) + \frac{\alpha_e h\nu}{C_e} J(t,z) \quad (1.1)$$

$$\frac{\partial T_a}{\partial t} = \alpha_a \frac{\partial^2 T_a}{\partial z^2} + \frac{1}{C_a \tau_{ep}}(T_e - T_a) \quad (1.2)$$

where $J(t,z)$ is the intensity distribution in the solid, $C_e = \frac{\pi^2 k_B^2 N_e}{2E_F}$ is the heat capacity of the electron gas, C_a is the heat capacity of atoms, τ_{ep} is the time of electron-phonon relaxation, T_e is the temperature of electrons, T_a is the temperature of atoms, α_e and α_a is the thermal diffusivity of electrons and ions; E_F is the Fermi energy; K_B is the Boltzmann constant.

For modelling the impact of the femtosecond laser radiation on the skin we used the following boundary conditions:

$$T_e|_{t=0} = T_e|_{t=0} = T_0 \quad (2.1)$$

$$\frac{\partial T_e}{\partial z}\Big|_{z=0} = \frac{\partial T_e}{\partial z}\Big|_{z=L} = \frac{\partial T_a}{\partial z}\Big|_{z=0} = \frac{\partial T_a}{\partial z}\Big|_{z=L} = 0 \quad (2.2)$$

Since the pulse duration is negligibly small ($\alpha_e \ll \frac{x^2}{t}$, $\alpha_a \ll \frac{x^2}{t}$, where x is the spatial representation of the pulse, and the heat diffusivity for a tissue $\alpha_a = 1.54 \times 10^{-3}$ cm^{2}s [15], and $\alpha_e < \alpha_a$), we can assume $\alpha_e \frac{\partial^2 T_e}{\partial z^2}$, $\alpha_a \frac{\partial^2 T_e}{\partial z^2} = 0$, and the function $\frac{\alpha_e h\nu}{c_e} \cdot J(t,z)$ can be replaced with the function $\Gamma\delta(z - vt)$, describing the heat source caused by the fast absorption of the radiation in the medium. The solution can be derived in the form:

$$T_e(t) - T_e(0) = \int_0^t (A + (1-A)exp(-\lambda(t-t'))) \cdot \Gamma\delta(z - vt')dt' \quad (3.1)$$

$$T_a(t) - T_a(0) = \frac{1}{\tau_{ep} \cdot c_e} \int_0^t (1 - exp(-\lambda(t-t'))) \cdot \Gamma\delta(z - vt')dt' \quad (3.2)$$

where $A = \frac{1}{C_e^2} + \frac{1}{C_e + C_a}$, $\lambda = \frac{1}{\tau_{ep}}(\frac{1}{c_e} + \frac{1}{c_a})$.

2.3 Results

By means of Monte Carlo numerical simulation of propagation of radiation through the skin tissues, we obtained the intensity distributions over the tissue depth (Fig. 2). The calculation approximated the solution of the radiation transfer equation by modelling all possible photon trajectories passing through the skin tissue model. The steady-state form of the radiation transfer equation in a homogeneous medium can be written as the integral equation [16, 17]:

$$L(r,s) = \int_{R-0}^{\infty} \exp(-\mu_{tr}R)\,\mu_s \int_{4\pi} p(s,s')L(r - Rs, s')d\,\Omega'\,\mathrm{dR} + \int_{R-0}^{\infty} \exp(-\mu_{tr}R)Q(r - Rs, s)dR \quad (4)$$

where L is the luminance at the point r in the direction s, considered for both the light source and for the radiation scattered towards the direction s; R is the path length, Q is the light emitted in the direction s by the source at the point r – Rs. The parameter $\exp(\mu_{tr}R)$ determines the radiation transfer from the point r – Rs to the point r. Thus, the first term in the equation characterises the light scattered at the point r – Rs, from any direction s' to the direction s, reaching the point r, and the second term describes the light emitted from the point r – Rs in the direction s.

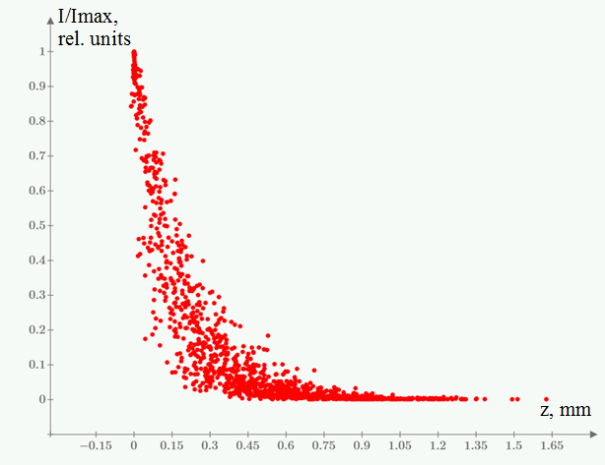


Fig. 2 Dependence of the radiation intensity upon the penetration depth (for λ = 800 nm).

From Fig. 2 one can see that at the depth of 0.3 mm the radiation intensity is less than 30% of the initial level. It is known that the probability of multiphoton processes is directly proportional the second, the third and higher powers of the laser intensity. Thus, the main nonlinear processes will take place in the upper skin layer, the epidermis.

The dynamics of the electron system can be described by the energy distribution. Figure 3 presents the energy distribution of electrons depending on the time passed after the pulse impact. The state of the

electron subsystem is shown immediately after the impact (a), after 1 ps, when a part of electrons has transferred their energy to the atom subsystem as a result of relaxation (b), and after more than 3 ps, when the most part of the electrons has transferred their energy to the atom subsystem, and the entire system tends to thermal equilibrium (c).

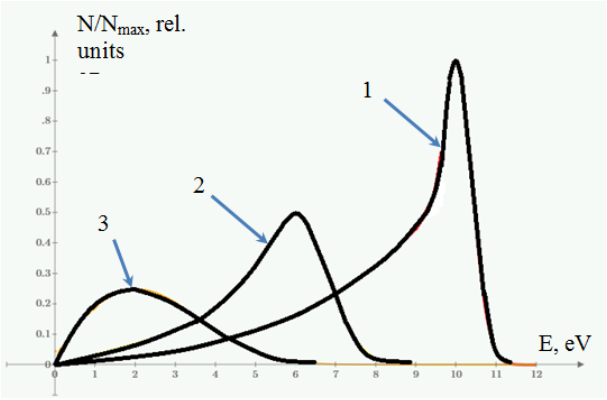


Fig. 3 Distribution of electrons over the energy levels depending upon time: 1 – the energy transfer to the electron subsystem, 2 and 3 – partial relaxation of electrons and transfer of the energy to the atomic subsystem.

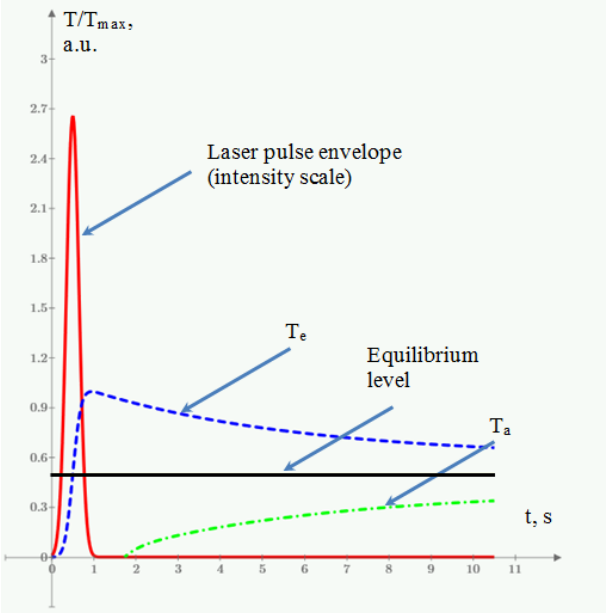


Fig. 4 Thermodynamics of the system. The laser pulse, dynamics of the electron gas temperature T_e and the crystal lattice temperature T_a.

The absorption of light quanta by nonequilibrium electrons of the dielectric increases their kinetic energy. This leads to the growth of electron temperature during the light pulse, whereas the lattice remains practically cold. Therefore, one can divide the process of the action of the femtosecond laser radiation on the skin into three stages. At the first stage during the femtosecond pulse the multiphoton excitation of water molecules occurs. The energy of ionisation in this process amounts to 6.5 eV, so that to ionise one water molecule nearly 5 photons (800 nm) are necessary, which is a cause for the reduction of the quantum efficiency ($\eta \leq 20\%$). Simultaneously the process of impact ionisation takes place. As a result, before the end of the laser pulse action $N_{max} \approx \eta \cdot E/\hbar w$ (E being the pulse energy) electrons will be excited to the upper ionised states of the water molecules with the energy above $U_i = 6.5$ eV. The second stage occurs after the action of the femtosecond pulse and lasts until the complete transfer of the energy from the electrons to the phonon subsystem. The electron gas is cooled and the collagen molecules are heated (tens of picoseconds). The third stage is the distribution of heat over the bulk sample (a few microseconds).

3 Conclusion

We presented a mathematical model of the propagation of femtosecond radiation through the cutaneous covering. Using the Mote Carlo numerical simulation, we determined the dependence of the radiation intensity upon the penetration depth. By the aid of the analytical solution of the system of equations describing the energy balance between the electron subsystem and the atomic one, we considered the mechanism of the effect of femtosecond radiation on the skin and estimated the temporal processes that occur in the course of the femtosecond radiation acting on the skin.

Acknowledgments

The results of this work were obtained within the framework of the State order №3.1675.2014/K from the Ministry of Education and Science of Russian Federation.

We also express our gratitude to Dr. Sergey A. Chivilikhin, Cand. Sci, staff member of the Photonics and Optoinformatics Chair of the ITMO University (Saint-Petersburg), for consultations and essential contribution to this work.

The use of laser dynamical speckle interferometry in the study of cellular processes

A. P. Vladimirov[1,2,3], I. A. Novoselova[1*], Y. A. Mikhailova[1,2], A. A. Bakharev[2], and D. I. Yakin[1]

[1] Ural Federal University named after the first President of Russia Boris N. Eltsin, Ekaterinburg, Russia
[2] Ekaterinburg Research Institute of Virus Infections, Ekaterinburg, Russia
[3] Institute of Engineering Science, Urals Branch, Russian Academy of Sciences, Ekaterinburg, Russia

[*] **e-mail:** inovoselova93@gmail.com

Abstract. A speckle interferometry setup is mounted, tested and approved that allows the analysis of intracellular processes with large optical magnification. For different part of the cell, the dependences of speckle image correlation coefficients upon time are found. It is shown that the method allows the detection of differences in the process that occur in the nutrient solution outside the cell and inside the cell, as well as those occurring in different parts of the cell. © 2016 Journal of Biomedical Photonics & Engineering.

Keywords: laser, speckle, speckle interferometry, cell metabolism, correlation.

Paper #2952 received 2016.01.31; revised manuscript received 2016.02.12; accepted for publication 2016.03.03; published online 2016.03.30. doi: 10.18287/JBPE16.02.010302

References

1. M. Francon, Laser Speckle and Applications in Optics, Academic Press, New York (1979). ISBN: 9780124337459.
2. V. V. Tuchin, Lasers and Optical Firbes in Biomedical Studies, 2nd ed., Fizmatlit, Moscow (2010) [in Russian].
3. V. P. Tychinskii, "Coherent phase microscopy of intracellular processes," Physics–Uspekhi 44(6), 617-629 (2001).
4. D. A. Zimnyakov, V. V. Tuchin, and S. R. Utz, "A study of statistical properties of partially developed speckle fields as applied to the diagnostics of structural changes in human skin," Opt. Spectrosc. 76, 838-844 (1994).
5. A. P. Vladimirov, A. L. Lisin, V. I. Mikushin, M. M. Kokhan, I. A. Kuklin, and E. V. Kononenko, "Biological activity of the human skin studied by method of speckle counting," Technical Physics Letters 26(5), 366-368 (2000).
6. G. G. Akchurin, V. V. Bakutkin, E. Y. Radchenko, and V. V. Tuchin, "Laser speckle interferometry and the possibility to determine the retinal acuity of vision in the case of cataract," Biomeditsinskiye tekhnologii i radioelektronika 1, 19-27 (2002) [in Russian].
7. Y. N. Dubnishchev, V. A. Arbuzov, and P. Y. Belousov, Optical Methods of Flow Studies, Novosibirsk ed., Sibirskoye universitetskoye izd-vo, Novosibirsk (2003) [in Russian].
8. A. P. Poryvaeva, and T. S. Nekrasova, "Cell cultures in the complex diagnostics of herpes virus infections," 6-ya regional'naya nauchno-prakticheskaya konferentsiya "Perpektivy ispol'zovaniya v meditsinskoy praktike novykh immunobiologicheskikh preparatov, poluchennykh na osnove kletochnykh struktur," May 30-31, Ekaterinburg, Sbornik materialov (2012).
9. V. V. Lychagov, A. L. Kalyanov, D. V. Lyakin, and V. P. Ryabukho, "Method for remote diagnostics of the internal structure of layered media," Quantum Electron. 38(6), 563–569 (2008).
10. A. P. Vladimirov, A. V. Druzhinin, A. S. Malygin, and K. N. Mikitas, "Theory and calibration of speckle dynamics of phase object," Proc. of SPIE 8337, 83370C (2012).
11. A. S. Malygin, N. V. Bebenina, A. P. Vladimirov, K. N. Mikitas, and A. A. Bakharev, "A speckle-interferometric device for studying the cell biological activity," Instruments and Experimental Techniques 55(3), 415–418 (2012).
12. N. V. Bebenina, "Application of dynamic speckle interferometry method to the study of metabolic activity of cells in the in vitro experiment," Master Thesis, Ekaterinburg (2012) [in Russian].

13. Y. A. Mikhailova, "Application of dynamic speckle interferometry to the analysis of metabolic activity of cultivated cells," graduate work, Ekaterinburg (2013) [in Russian].
14. N. P. Glinskikh, V. N. Avdeeva, F. Y. Zusman, et al., Patent No. 2148644 of Russian Federation.

1 Introduction

The progress in cell technologies makes it particularly important to develop the method of noninvasive control of the cell physiological condition. For this aim, the indirect techniques are mainly applied, based on the examination of the products discharged from the cell in the course of metabolism, which is not always adequate to the real cell vital activity. At present, there are a few basic methods of cell investigation, e.g., light microscopy, phase-contrast microscopy, fluorescence microscopy, electron microscopy, autoradiography, centrifuging, freezing-spalling techniques. All these methods are rather labour and time consuming, require careful preparation of samples, which makes the full-scale diagnostics of living cells unpractical.

Promising for studying the living cell activity are the optical coherence methods based on the use of lasers. The laser radiation of moderate intensity exerts non-specific thermal action on biological objects, while the high-intensity laser radiation destroys the biological objects, manifesting itself like other electromagnetic radiations of different nature. However, at relatively low intensities it appears possible to use light for studying the processes in a living object without introducing any serious disturbance of its behaviour. The region of extremely small intensities is of interest, in which it is possible to apply a number of most sensitive methods that do not require strong light fluxes and, therefore, do not introduce distortions into the measurement results due to the homeostasis of living matter even at the local level.

It follows that the extension of the use of optical methods, including the coherence optical ones, in the control of the object condition and diagnostics is caused by the availability, high speed, clearness of information, with the possibility to provide high accuracy of the measurements. Besides the comparability of the optical wavelength with the elements of the controlled object microstructure and the interference of multiple waves allow the possibility to study the object structures at the microscopic level.

In the present paper in order to study the micro- and macroscopic processes that occur in cells, we apply the method of recording the dynamics of laser speckles, or biospeckles. At present, the biospeckles are successfully used to study the activity of different biological objects [1-8]. Earlier the dynamics of speckles was already used to estimate the biological activity of seeds, human skin, and other objects. One of the most successful examples of using the biospeckles is the development of the approach, in which by the contrast of the speckles the blood flow velocity at the eye retina and in near-surface cutaneous coverings of a patient's limb were assessed. At present, the method is well developed both theoretically and experimentally. In Ref. [9] the method of autocorrelation low-coherence interferometry is considered for using in the studies of optical inhomogeneities and internal structure of layered media of technical and biological origin that allows the study of layered objects, among which a cell can be considered, but this method is also capable of analysing the structure and the shape of an object. The present paper is aimed at the study of the processes in real time that occur in the cell membranes and in the cells themselves, which is an urgent problem from both the academic and the practical point of view.

The urgency of such studies is due to the fact that human diseases are directly or indirectly related to the failure of normal functioning of cells or biological membranes. Many diseases are caused by modifications of the structure and functional properties of the cell molecular components under the action of either the external factors or the internal disorders.

In Ref. [10] the theoretical justification of the method was given and the calibration was implemented. In Ref. [11] the parameter characterising the metabolic activity of cells was chosen and justified. The authors of Ref. [12] demonstrated the possibility to study the interaction of herpes with cell cultures and in Ref. [13] the technique was upgraded to obtain stable and reproducible results.

In the above papers, the determination of the parameter characterising the cell metabolic activity was implemented by evaluating the degree of correlation between two speckle patterns. The correlation of speckle patterns was recorded in two areas. The first area was chosen in the image of cells and the second one beyond this image. The technique was developed that allowed one to determine the quantity characterising the cell metabolic activity from two values of the degree of correlation of the image areas. It was shown that such quantity is the root-mean-square deviation of the optical path difference for the pairs of waves, probing the cell.

In all above papers, a few cells could be placed in the area, the linear size of which equals the lens linear resolution. The determination of the parameter characterising the metabolic activity was implemented by averaging over hundreds of cells. However, the logics of the method development required the investigation of the phenomena that occur within a single cell near the membrane, in the cytoplasm or the nucleus.

The aim of this work was to create a speckle interferometric setup for the analysis of intracellular processes under high optical magnification, as well as the study of the change of the parameter characterising the degree of correlation of two speckle patterns, recorded inside and outside individual cells.

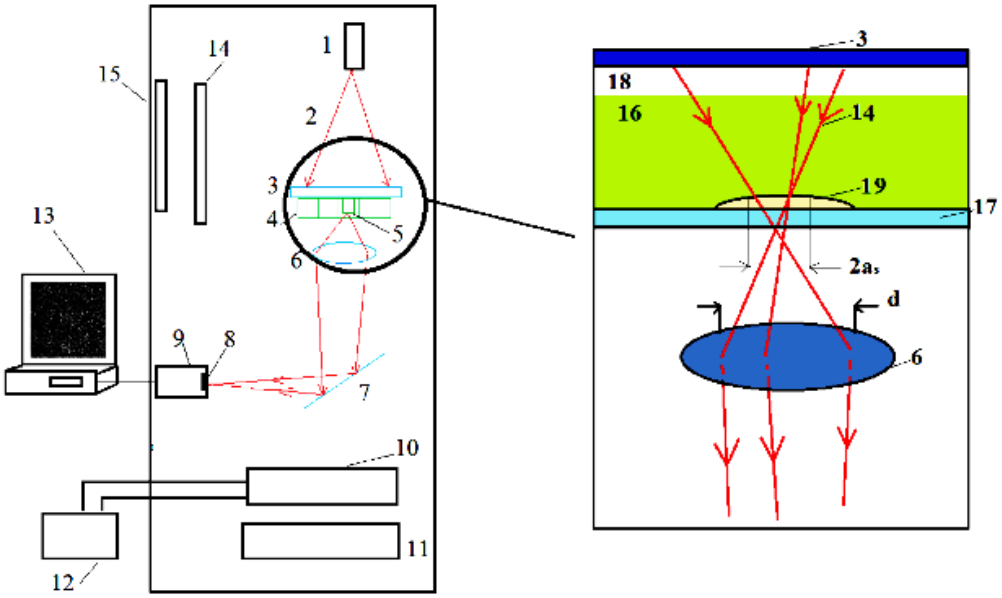
As compared to the analogues, the main advantage of the setup is its high sensitivity. The existing methods and instruments use the double beam interference of waves, and in our system the interferometry of multiple waves is implemented, therefore the sensitivity of the method is by 1-2 orders of magnitude higher than in the analogues. This offers new possibilities in the study of intracellular processes for developing novel methods of diagnostics and complex treatment of various diseases.

2 Speckle interferometric setup

We designed and mounted the setup, the general view of which is presented in Figure 1. The optical scheme of the device is presented in Figure 2.



Fig. 1 Photograph of the experimental setup.



1 – laser, 2 – coherent radiation, 3 – diffuser, 4 – sectioned cuvette, 5 – section with cell culture, 6 – microscope lens, 7 – mirror, 8 – array of photodetectors, 9 – TV camera, 10 – radiator, 11 – fan, 12 – thermostat, 13 – notebook, 14 – thermometer, 15 – window, 16 – nutrient solution, 17 – cuvette bottom, 18 – air medium, 19 – cell; 2as – linear magnification of the microscope, d – microscope lens aperture diameter.

Fig. 2 Schemes of the optical setup and ray paths.

The authors of Ref. [2] report that the cell viability is observed even under the 300 seconds exposure with the light at the wavelength 660 nm with the power 20 mW, the beam cross section area being nearly 0.25 μm^2 (the power density 8 mW/cm^2). In the present study as the source of light 1 we used the semiconductor laser unit with the wavelength λ=0.65 μm and the power 20 mW, the power density being 2.1 mW/cm^2. The radiation from the laser was incident on the diffuser 3 and passed through the cuvette 4 with the studied sample. The cuvette bottom with cells sediment was separated from the diffuser by nearly 10 mm. Then the radiation arrived at the objective 6 with the aperture providing the formation of speckle pattern. In the experiments, we used a monochrome TV camera Videoscan-415/P/K-USB. The camera had an array of photodetectors 6.5×4.8 mm with 780×582 pixels, each having the dimensions 8.3×8.3 μm. The frame repetition rate was up to 25 Hz. The TV camera exposure time was 9 seconds, which exceeded the correlation time of

radiation intensity (5-8 seconds), corresponding to the most rapid processes [10].

The optimal temperature for the cell culture growth is known to be 36.6 ± 0.5^0C, and the decrease of the temperature leads to immediate reduction of the cell physiological activity. Therefore, the system was placed in a thermostat 12. The signals from the TV camera via the USB port were transmitted to the Aspire 3692 WLMi (Acer) notebook 13.

The calibration of the instrument was implemented using a thin plate with the roughness parameter Ra about 10 nm. The procedure of calibration is rather simple and described in [10].

2.1 Software

To enter the image frames we used the «Viewer» software supplied together with the VideoScan camera. The Program has options that allow the recording of individual frames, as well as the movies of speckle dynamics. The frames are recorded in the bmp format. The program allows setting the signal amplification, the frame exposure time, and controlling the rate of the input frames.

Further processing of the experimental data was implemented using the standard packages of Microsoft Excel 2010.

2.2 Technique of experiment and processing of the results

The nutrient solution with cells was placed in the cuvette. The cuvette was covered with the diffuser and put into the setup, where the thermostat kept the temperature equal to 36°C. To measure the temperature in the setup the thermometer was used.

Using the special software, we recorded the values of the parameter η, characterising the cell metabolic activity and calculated using the formula:

$$\eta = \frac{\frac{1}{m \cdot n}\sum_{i=0}^{m-1}\sum_{j=0}^{n-1}[A_{i,j} - \bar{A}\,][B_{i,j} - \bar{B}\,]}{\sqrt{\frac{1}{m \cdot n}\sum_{i=0}^{m-1}\sum_{j=0}^{n-1}[A_{i,j} - \bar{A}\,]^2} \cdot \sqrt{\frac{1}{m \cdot n}\sum_{i=0}^{m-1}\sum_{j=0}^{n-1}[B_{i,j} - \bar{B}\,]^2}}, \qquad (1)$$

where $A_{i,j}$ are the signals in the area of $m \times n$ pixels at the initial moment of time, $B_{i,j}$ are the signals from the same area at a different moment of time τ, *i, j* are the pixel numbers in the *x* and *y* directions, respectively, $\bar{A}$ is the mean values of the signals for the area at the initial moment of time, $\bar{B}$ is the same mean value at the time moment τ.

2.3 Object of study

As the object of study, we took the cell cultures L-41 KD/84. The cell culture L-41 is a cancer culture. The specialists from the Ekaterinburg Research Institute of Virus Infections performed the preparation of biological samples.

According to the certificate of the cell line L-41 KD/84 [13], the strain of transferred cells G-96 is known to be extracted from the blood of a patient suffering from monocytic leukaemia. In 1966 V.D. Solovyov et al. subjected it to triple impact of large doses of the Koksaki B3 virus to obtain the subline (G-41), specifically resistant to this virus. The clone line L-41 KD/84 was obtained in 1984 in the Laboratory of Cell Cultures, the Ekaterinburg Research Institute of Virus Infections, using the Puck double cloning method with subsequent treatment with antibiotics.

Morphologically the cell line L-41 is a uniform monolayer of distinct epithelium-like polygonal or rounded cells, among which 4-6% of gigantic cells are permanently present. The cytoplasm is fine-grained. The nuclei are rounded and contain 2-4 nucleoli. The anomalous mitosis forms are up to 6 % and the number of cell with irregular shape of nuclei is up to 8%. The monolayer is formed in 3-5 days from the moment of seeding in the medium, consisting of equal volumes of the “Igla” and “199” media with the addition of 10% bovine embryo serum. The cell maintenance medium contains the necessary amino acids, vitamins, salts, and glucose.

The culture is highly sensitive to viruses of poliomyelitis, Koksaki B, ECHO-19, human adenoviruses, and the measles virus. The mean cell size is 20-30 μm.

3 Results and discussion

Figure 3 presents a typical speckle pattern observed at a certain fixed moment of time at the computer monitor. One can easily distinguish the cells of the L-41 culture that appeared to be deposited on the substrate during one hour. The frame exposure time was equal to 9 seconds.

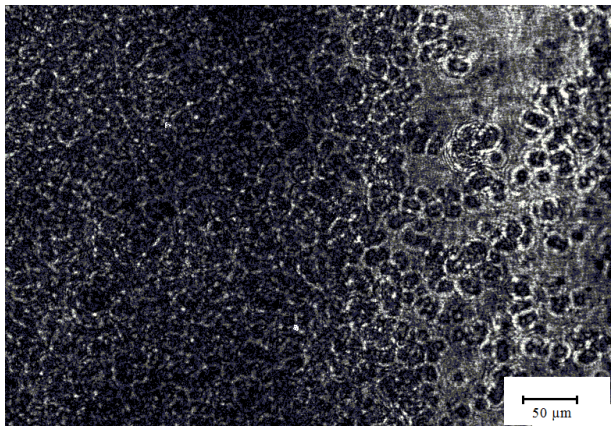


Fig. 3 Speckle pattern for the cell culture L-41.

The performed observations have shown that the cells are not stable. The changes occur both inside each cell and in the entire cell array. We managed to select a few cells, which among others could be considered as visually immobile during an hour. Figure 4 presents a typical dependence η=η(t) for a stable cell. The value of

the parameter η was found by averaging over the area, the size of which was nearly equal to that of a cell.

For stable cells we determined also the autocorrelation function η=η(t) for small regions in the cell image. The size of the regions was 5×5 pixels. Figures 5 and 6 present typical autocorrelation functions of the regions near the cell edge and in the centre of the cell, respectively.

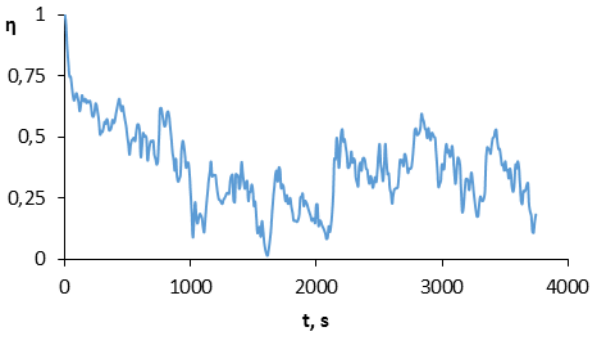


Fig. 4 Typical autocorrelation function for a stable cell.

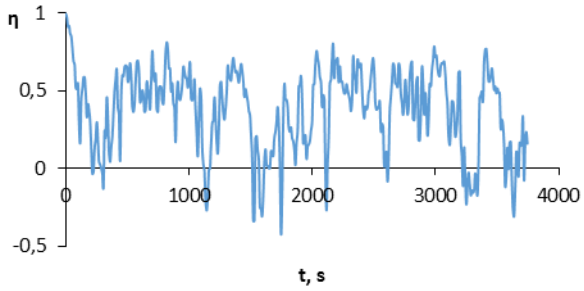


Fig. 5 Typical autocorrelation function for a region inside the stable cell image near the edge.

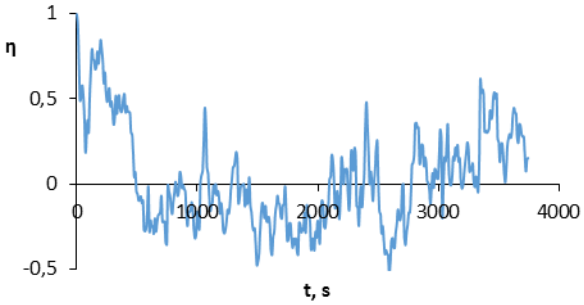


Fig. 6 Typical autocorrelation function for a region inside the stable cell image near the centre.

Figure 7 presents typical autocorrelation functions, corresponding to individual unstable cells. The size of the studied regions was 20×20 pixels.

The analysis of the obtained data has shown that if the size of the region of averaging is greater of equal to that of a single cell, then for stable cells the autocorrelation function varies within the limits from 0 to 1, while for unstable cells η can take both positive and negative values.

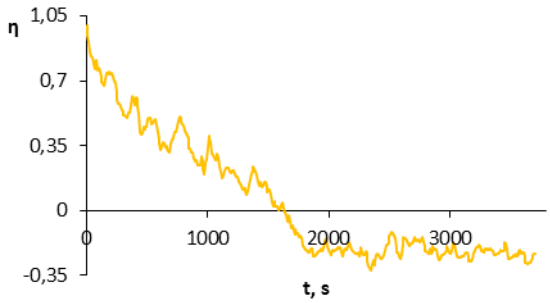


Fig. 7 Typical autocorrelation function of unstable cells.

Using the speckle interferometric setup we also performed the experiment with relatively small number of cultivated cells in the nutrient solution. The object of study was not a monolayer, but individual cells with the typical separation of 2-5 μm between them. Figure 8 presents the dependences η=η(t) for different regions of the cell image and the dependence η=η(t) for the nutrient solution

As seen from Fig. 8, the value of η for the region outside the cell varies within the limits from 0.95 to 0.99, while for the region inside the cell the variation occurs with the limits from 0.2 to 0.99.

Thus, from the presented data one can see that the setup and the method allow the distinction of processes that occur in the nutrient solution and in the cells.

The autocorrelation functions plotted above were calculated in small regions in different cell parts, as well as by averaging over the entire cell. For immobile cells, one can see that the correlation coefficient, corresponding to intracellular regions, can take both positive and negative values. However, in the case of a separate stable cell, the values of the correlation coefficients are only positive, and this is an important result. For an unstable cell, the values of the correlation coefficient can be positive and negative in the case of averaging over a single cell. This is probably due to the cell displacements. The clarification of this issue is a subject of further study. The aim of the present analysis was to present new experimental results. In future, the authors plan to analyse the experimental results with the attraction of theory.

In Ref. [11] the formula is presented that relates the correlation coefficient η and the root-mean-square deviation of the optical path lengths for pair of waves. According to this formula the obtained value of η=0.99 corresponds to the root-mean-square deviation of optical paths of the order of 1 nm.

Thus, the authors have shown that the present technique allows the analysis of the variation of the optical path difference of wave pairs, averaged over the region with the size of a few micrometres. The drawback of the methods at present is the averaging of the data over the cell thickness. Therefore, further studies are required on the development of living cell tomography in order to get information on the processes with the depth resolution. Besides that, the method is applicable to relatively slow processes.

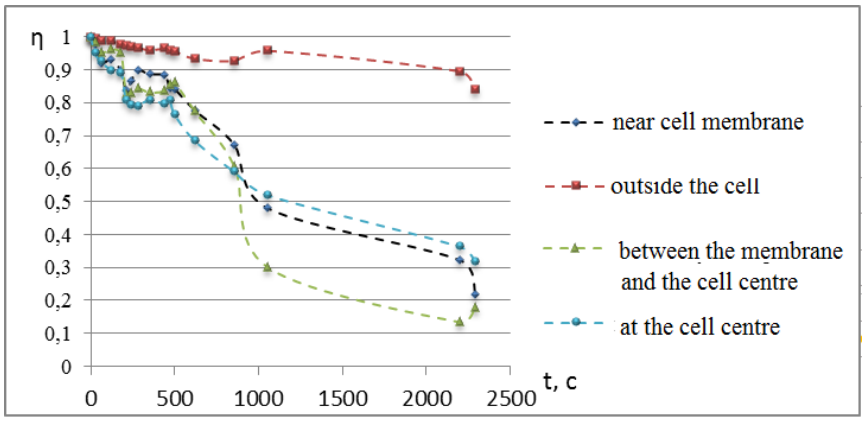


Fig. 8 Dependence η=η(t) outside and inside the cell.

4 Conclusion

Basing on the obtained data, one can draw the following conclusions:

1. The speckle interferometer that allows the determination of speckle dynamics parameters in small regions inside the images of individual cells with overall magnification to 320× is designed and successfully approved.
2. As a diagnostic parameter, the correlation coefficient for one fragment of speckle pattern taken at two different moments of time is chosen.
3. It is shown that the interferometer allows the registration of the distribution of this parameter within the cell image and beyond it.
4. The difference of the speckle dynamics parameters is revealed between the regions in the cell and outside it, as well as between different regions within one cell image.

The obtained data form a basis for the improvement of the technique. The authors plan to increase the operation rate of the setup and to achieve the temporal resolution of 1 μs.

Ex vivo investigation of glycerol diffusion in skin tissue

Vadim D. Genin[1*], Daria K. Tuchina[1], Ali Jaafar Sadeq[1], Elina A. Genina[1,2], Valery V. Tuchin[1,2], and Alexey N. Bashkatov[1,2]

[1] N.G. Chernyshevsky Saratov State University, 83 Astrakhanskaya Str., Saratov 410012, Russia
[2] Tomsk State University, 36 Prosp. Lenina, Tomsk 634050, Russia

[*] **e-mail:** versetty2005@yandex.ru

Abstract. The change of optical parameters of rat skin *ex vivo* under the action of aqueous 30%, 50%, 60%, 70%, 85%, and 100% glycerol solutions has been experimentally studied. The analysis of kinetics of the change of the studied parameters has allowed the estimate of the diffusion coefficient dependence upon the concentration of glycerol in the skin and the efficiency of optical clearing for each of the glycerol solutions. The results can find application in the development of new methods of noninvasive diagnostics and therapy of skin diseases. © 2016 Journal of Biomedical Photonics & Engineering.

Keywords: glycerol, diffusion coefficient, skin, optical clearing.

Paper #2933 received 2016.01.19 revised manuscript received 2016.03.10; accepted for publication 2016.03.10; published online 2016.03.29. doi: 10.18287/JBPE16.02.010303

References

1. V. V. Tuchin, Tissue optics: Light Scattering Methods and Instruments for Medical Diagnosis. Third edition, SPIE Tutorial Text in Optical Engineering, SPIE Press, Washington, Bellingham (2015). ISBN: 9781628415162
2. E. A. Genina, A. N. Bashkatov, and V. V. Tuchin, "Tissue optical immersion clearing," Expert Review of Medical Devices 7(6), 825-842 (2010).
3. D. Zhu, K. Larin, Q. Luo, and V. V. Tuchin, "Recent progress in tissue optical clearing," Laser & Photonics Reviews 7(5), 732-757 (2013).
4. E. A. Genina, A. N. Bashkatov, Y. P. Sinichkin, I. Y. Yanina, and V. V. Tuchin, "Optical clearing of biological tissues: prospects of application in medical diagnostics and phototherapy," Journal of Biomedical Photonics & Engineering 1(1), 22-58 (2015).
5. C. G. Rylander, O. F. Stumpp, T. E. Milner, N. J. Kemp, J. M. Mendenhall, K. R. Diller, and A. J. Welch, "Dehydration mechanism of optical clearing in tissue," J. Biomed. Opt. 11(4), 041117 (2006).
6. A. T. Yeh, and J. Hirshburg, "Molecular interactions of exogenous chemical agents with collagen-implications for tissue optical clearing," J. Biomed. Opt. 11(1), 014003 (2006).
7. E. A. Genina, A. N. Bashkatov, Y. P. Sinichkin, and V. V. Tuchin, "Optical clearing of skin under action of glycerol: ex vivo and in vivo investigations," Optics and Spectroscopy 109(2), 225-231 (2010).
8. M. A. Fox, D. G. Diven, K. Sra, A. Boretsky, T. Poonawalla, A. Readinger, M. Motamedi, and R. J. McNichols, "Dermal scatter reduction in human skin: a method using controlled application of glycerol," Lasers Surg. Med. 41, 251-255 (2009).
9. T. Son, and B. Jung, "Cross-evaluation of optimal glycerol concentration to enhance optical clearing efficacy," Skin Research and Technology 21(3), 327-332 (2015).
10. E. Youn, T. Son, H.-S. Kim, and B. Jung, "Determination of optimal glycerol concentration for optical tissue clearing," Proc. SPIE 8207, 82070J (2012).
11. J. B. Segur, and H. E. Oberstar, "Viscosity of glycerol and its aqueous solutions," Ind. and Eng. Chem. 43(9), 2117-2120 (1951).
12. A. N. Bashkatov, E. A. Genina, and V. V. Tuchin, "Measurement of glucose diffusion coefficients in human tissues," Chapter 19 in Handbook of Optical Sensing of Glucose in Biological Fluids and Tissues, V. V. Tuchin (Ed.), Taylor & Francis Group LLC, CRC Press, 587-621 (2009).

13. D. K. Tuchina, R. Shi, A. N. Bashkatov, E. A. Genina, D. Zhu, Q. Luo, and V. V. Tuchin, "Ex vivo optical measurements of glucose diffusion kinetics in native and diabetic mouse skin," J. Biophotonics 8(4), 332-346 (2015).
14. Y. Nishijima, and G. Oster, "Diffusion of glycerol-water mixture," Bulletin of the Chemical Society of Japan 33(12), 1649-1651 (1960).
15. B. Chen, E. E. Sigmund, and W. P. Halperin, "Stokes-Einstein relation in supercooled aqueous solutions of glycerol," Phys. Rev. Lett. 96(14), 145502 (2006).
16. W. Chen, J. Jiang, W. Zhang, R. K. Wang, and K. Xu, "Typical application of skin diffusion optical model to quantitative description of tissue optical properties," Proc. SPIE 7176, 71760L (2009).
17. D. Huang, W. Zhang, H. Zhong, H. Xiong, X. Guo, and Z. Guo, "Optical clearing of porcine skin tissue in vitro studied by Raman microspectroscopy," J. Biomed. Opt. 17(1), 015004 (2012).
18. J. Jiang, L. Zhang, and R. K. Wang, "Synergistic effect of hyperosmotic agents under topical application on optical clearing of skin tissue in vitro," Proc. SPIE 5696, 80-90 (2005).
19. Z. Mao, Z. Han, X. Wen, Q. Luo, and D. Zhu, "Influence of glycerol with different concentration on skin optical clearing and morphological changes *in vivo*," Proc. SPIE 7278, 72781T (2009).
20. X. Xu, and Q. Zhu, "Feasibility of sonophoretic delivery for effective skin optical clearing," IEEE Transactions on Biomedical Engineering 55(4), 1432-1437 (2008).

1 Introduction

Optical methods of diagnostics and treatment of different diseases are now widely used in medicine due to their relatively low cost and harmlessness for the patient's health. One of the important problems faced by the modern laser medicine is the transport of radiation to deeper tissue layers. Significant light scattering in tissues, particularly in skin, in the visible and near-infrared spectral ranges seriously restricts the spatial resolution and probing depth of the used methods [1]. One of the possible ways to solve this problem is to reduce the light scattering by partial replacement of the interstitial fluid with various immersion agents, i.e., to make use of the so-called optical clearing technique [1-4].

The method of tissue optical clearing consists in matching the refractive indices of its components by partial replacement of the interstitial fluid with a biocompatible optical clearing agent (OCA) [1-4]. At present, three mechanisms are proposed to explain the reduction of light scattering under the effect of OCA, namely, the osmotic dehydration of the tissue, the replacement of interstitial fluid with the agent matching the refractive indices of the tissue components, and the structure modification or dissociation of the tissue collagen [1-4]. In real situations the first two mechanisms usually manifest themselves together. The difference, caused by the type of OCA and the tissue, will consist only in the relative contribution of each mechanism into the clearing effect. The influence of the third mechanism on the degree of clearing becomes noticeable only in the case of long-term action of hyperosmotic immersion liquids on the tissue [4].

The aqueous solutions of glycerol are immersion liquids widely used as OCAs due to their efficiency, availability, and biocompatibility [1-8]. Unfortunately, in spite of the wide use of glycerol for controlling the tissue optical parameters, there is no unambiguous answer to the question about the optimal concentration of the glycerol solution. Although the literature data [9, 10] allow the conclusion on the most efficient concentration of the glycerol solution from the point of view of the optical clearing degree, the concentration dependence of the glycerol diffusion coefficient in tissues remains to be an open issue.

The knowledge of the diffusion coefficients and the mechanisms of interaction of the studied OCAs with tissues are necessary for the development and optimization of the tissue optical clearing methods. Therefore, the aim of the present paper is to study the concentration dependence of the diffusion coefficient of glycerol in skin and the dependence of the skin optical clearing efficiency upon the glycerol concentration in the immersion clearing solution.

2 Materials and methods

As an object of study we used 60 samples of skin of white laboratory rats *ex vivo* (10 samples for each of the six clearing solutions). The hair was removed using the depilatory cream «Veet» (Reckitt Benckiser, France). The size of the samples was nearly 10×15 mm^2. The thickness of the samples was measured before the beginning of the experiment at five points by means of a micrometer with the accuracy ±5 μm, the results were averaged.

As OCAs we used the aqueous 30%, 50%, 60%, 70%, 85%, and 100% solutions of glycerol, prepared by dissolving (in volume fractions) the dehydrated glycerol (REACHEM, Russia) with distilled water. The refractive indices of the agents, measured by means of the Abbe refractometer IRF-454-B2M (LOMO, Russia) at the wavelength 589 nm, are presented in Table 1. The measurement error is ±0.0001.

The method of assessing the diffusion coefficients of immersion liquids in tissues, based on measuring the time dependence of collimated transmission in tissue samples, merged in the solution of clearing liquid, is thoroughly described in Refs. [12, 13].

Table 1 Refractive indices and viscosity of the glycerol solutions with different concentrations.

Concentration of glycerol solution	Refractive index of the solution	Viscosity of aqueous solutions of glycerol, mPa×s [11]
30%	1.378	2.5
50%	1.399	6
60%	1.415	10.8
70%	1.428	22.5
85%	1.452	109
100%	1.472	1410

In the study of the interaction between the glycerol solutions and the skin samples it was assumed that only the refractive index of the interstitial fluid is changed due to the diffusion of the immersion liquid into the sample and the osmotic dehydration of the tissue. In the course of diffusion of the substance with the refractive index greater than that of the interstitial fluid into the tissue and the efflux of water from the tissue, the matching of the refractive indices of scatterers and interstitial fluid occurs, which leads to the reduction of the scattering coefficient of the tissue. Studying the kinetics of this process allows the estimation of the diffusion coefficient as a measure of the mean exchange flow rate of the hyperosmotic liquid into the tissue and of water from the tissue.

The maximal efficiency of the skin optical clearing (efficiency factor) was calculated using the formula

$$OC_{eff} = \frac{\mu_t(t=0) - \mu_t^{\min}}{\mu_t(t=0)}, \qquad (1)$$

where μ_t is the attenuation coefficient calculated from the measured time dependence of the collimated transmission using the Bouguer-Lambert law; $\mu_t^{\min}$ is the minimal value of the attenuation coefficient.

The values of diffusion coefficient and the efficiency of optical clearing were calculated using the specially elaborated computer program for each wavelength and then averaged. The values of the diffusion coefficient were averaged over 10 samples for each of the studied concentrations of glycerol. The averaging of the optical clearing efficiency factor was also carried out over 10 samples for each of the studied concentrations of glycerol, but the values were grouped in three spectral regions, 500-600 nm, 600-700 nm, and 700-900 nm.

To measure the collimated transmission, we used the setup, consisting of the radiation source, namely, the halogen lamp HL-2000 (Ocean Optics, USA) (1), the optical fibres P400-1-VIS-NIR (Ocean Optics, USA), transporting the radiation to the tissue sample (2) and collecting the radiation passed through the sample (4), the cuvette with the sample (3), the spectrometer USB4000-Vis-NIR (Ocean Optics, USA) (5), and the computer (6) (Fig. 1).

For measuring the collimated transmission, the tissue samples were fixed in the plastic holder having the dimensions 38×17 mm^2 with the 8×8 mm^2 window and were put into the glass cuvette with 5 ml of glycerol solution, placed between two optical fibres with the inner diameter 400 μm. To provide the beam collimation, the collimators 74-ACR (Ocean Optics, USA) were fixed at the faces of the fibres by means of the standard connectors SMA-905.

The kinetics of the collimated transmission variation was recorded by sequential recording of the transmission spectra in the range 500-900 nm every 3-5 minutes during 1-2 hours. All measurements were performed at room temperature (~20°C).

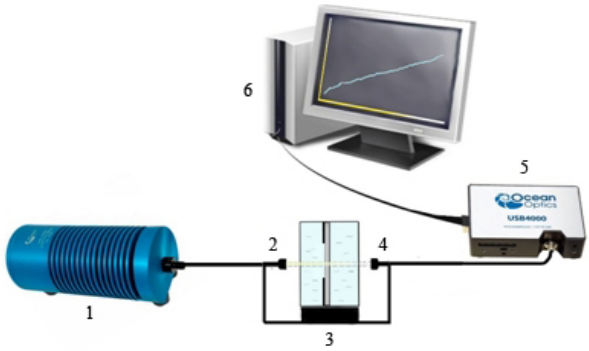
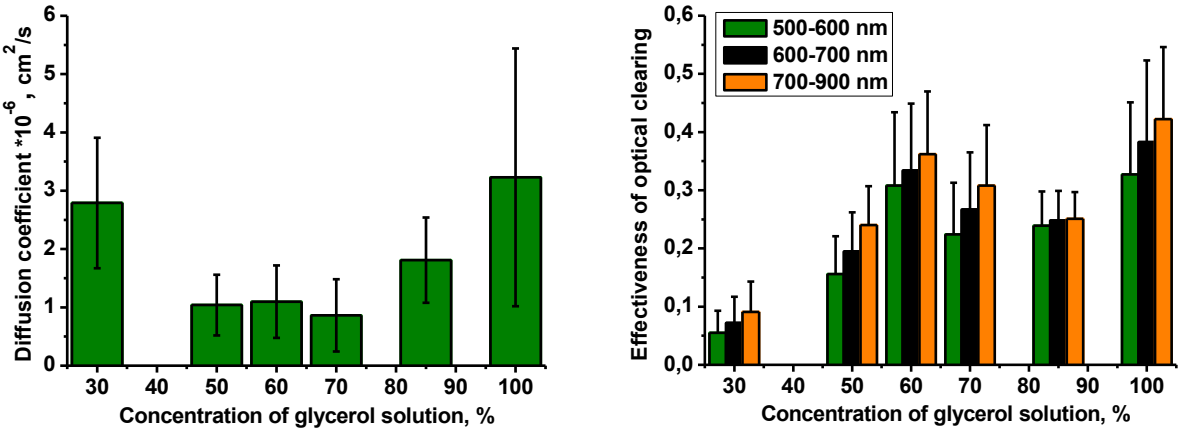


Fig. 1 Experimental setup: 1 - halogen lamp HL-2000; 2, 4 - optical fibres P400-1-VIS-NIR with collimators 74-ACR at the faces; 3 - cuvette with glycerol solution and skin sample, fixed in the frame; 5 - USB4000-VIS-NIR spectrometer; 6 – PC.

3 Results and discussion

Figure 2(a) presents a diagram illustrating the dependence of the diffusion coefficient of glycerol in skin upon the concentration of the glycerol solution. One can clearly see that the diffusion coefficient at first decreases till the concentration reaches 70% and then grows. This observation correlates well with the concentration dependence of the diffusion coefficient for glycerol in water [14] and is explained by both the increase of viscosity of the diffusing solution and the specific features of the formation of hydrodynamic radius of the diffusing molecules. As shown in Ref. [14], the hydrodynamic radius of glycerol molecules for the concentrations from 0 to 70% weakly depends on the glycerol concentration and decreases for higher concentrations, which is confirmed by the data of Ref. [15].

Thus, in the optical clearing of skin with the aqueous solutions of glycerol with the concentration 30-70% the reduction of the glycerol diffusion rate is due to the growth of the viscosity of the diffusing solution. For high-concentration glycerol solutions (85-100%) there are two competing processes, the sharp increase of the diffusing solution viscosity and the decrease of the hydrodynamic radius of the glycerol molecules. As seen from Fig. 2(a), the contribution of the second process appears to be dominant, and we observe the growth of



(a) (b)

Fig. 2 Values of the diffusion coefficient (a) and optical clearing efficiency factor for the rat skin ex vivo in three different spectral ranges (b) depending on the concentration of solution. Bars correspond to the standard deviation.

Table 2 Values of the diffusion coefficient of glycerol in skin and the efficiency factor of the skin optical clearing.

Glycerol solution concentration	Skin samples thickness, mm	Efficiency of optical clearing in the region 500-600 nm	Efficiency of optical clearing in the region 600-700 nm	Efficiency of optical clearing in the region 700-900 nm	Diffusion coefficient, cm^2/s
30%	0.60±0.08	0.055±0.038	0.072±0.045	0.091±0.052	$(2.79\pm1.12)\times10^{-6}$
50%	0.38±0.11	0.156±0.065	0.195±0.067	0.240±0.067	$(1.04\pm0.52)\times10^{-6}$
60%	0.32±0.10	0.308±0.126	0.334±0.115	0.362±0.108	$(1.098\pm0.62)\times10^{-6}$
70%	0.48±0.07	0.224±0.089	0.267±0.098	0.308±0.104	$(0.86\pm0.73)\times10^{-6}$
85%	0.57±0.16	0.239±0.059	0.248±0.051	0.251±0.046	$(1.81\pm1.13)\times10^{-6}$
100%	0.46±0.13	0.327±0.124	0.383±0.14	0.422±0.124	$(3.23\pm2.21)\times10^{-6}$

the diffusion coefficient. Besides, as mentioned above, the coefficient of diffusion measured in the present work is a measure of the mean rate of the total exchange flow of the hyperosmotic liquid (glycerol solution) into the tissue and the water from the tissue. Correspondingly, for more correct determination of the diffusion coefficient of glycerol in the tissue one has to separate these processes from each other, which will be the aim of our further studies.

Table 2 presents the calculated diffusion coefficients for each of the glycerol solutions, as well as the efficiency coefficients of the skin optical clearing, grouped over three spectral ranges. Large values of the standard deviation for the determined values of the diffusion coefficients are due to the natural spread of the optical, structural, and morphological parameters of the skin samples.

Figure 2(b) shows the dependence of the skin optical clearing efficiency upon the concentration of glycerol solutions. From Fig. 2(b) it follows that the larger value of the OCA diffusion coefficient does not ensure the higher efficiency of the tissue optical clearing. Among the studied OCAs, in spite of the high rate of penetration into the tissue, the lowest efficiency of the optical clearing is observed in the 30% glycerol solution. This is because although the 30% glycerol solution is a liquid with the minimal viscosity, it also possesses the minimal refractive index.

The growth of the efficiency coefficient of the skin optical clearing in the case of using the glycerol solutions with concentrations of 30-60% as OCAs is explained by the increased matching of the OCA refractive index (1.378 for 30% solution and 1.415 for 60% solution) to that of the collagen fibres (1.411-1.416 [1]), which are the main scatterers in the skin. Then the efficiency of optical clearing decreases because the refractive index of OCA becomes greater than that of the collagen fibres. These results correlate well with the data, presented in Refs. [9, 10, 16-20], where the optical transmission of skin increased with the growth of the concentration of glycerol solution in the ranges 30-80% [16], 40-80% [17], 50-80% [18], 20-55% [19], 40-80% [20].

Similar results are demonstrated also in Refs. [9, 10], where the glycerol solution concentrations from 50 to 90% were used, and it was shown that the maximal efficiency of clearing is observed for the 70% solution, while for smaller or greater concentrations the clearing efficiency significantly decreases.

For the concentrations of the glycerol solution from 85% to 100% the efficiency of optical clearing increases again. Probably, this fact is due to the dominant role of

the dehydration mechanism of the optical clearing: the dehydration of the skin leads to the reduction of its thickness and, therefore increases the collimated transmission. Probably, the refractive index of collagen fibres is increased due to the destruction of their hydrate shells, leading to better matching of refractive indices of skin scatterers and their environment, the role of which in this case is played by the nigh-concentration glycerol solution. However, this hypothesis requires further studies.

4 Conclusion

The obtained results allow one to estimate the efficiency of using aqueous glycerol solutions with different concentrations as clearing agents controlling the scattering properties of skin. The most efficient optical clearing within the spectral range 500-900 nm was demonstrated with the 60% and 100% solutions of glycerol. Sufficiently high diffusion rate in combination with high efficiency of optical clearing was demonstrated by the 85% solution of glycerol.

Acknowledgments

The work was carried out under the financial support from the Russian Science Foundation, grant No. 14-15-00186.

Diagnostics of liquid properties by the example of bioorganic solutions

Alexander Malov, Anna Neupokoeva*, Alexandra Sambyalova
Department of Medical and Biological Physics, Irkutsk State Medical University, Irkutsk, Krasnogo Vosstaniya Str. 1, 664009, Russia

* **e-mail:** annett_2005@inbox.ru

Abstract. Two methods of monitoring the structure modifications of protein solutions are considered: using the speckle patterns in real time and using crystallograms. It is shown that the proposed methods of image processing correlate with each other and allow the tracing of the qualitative structure modifications. © 2016 Journal of Biomedical Photonics & Engineering.

Keywords: speckle, crystallogram, image processing, contour, structure monitoring, autocorrelation.

Paper #2889 received 2016.01.08; revised manuscript received 2016.03.02; accepted for publication 2016.03.09; published online 2016.03.30. doi: 10.18287/JBPE16.02.010304

References

1. A. N. Malov, and A. V. Neupokoyeva, "Chess board method for the analysis of speckle images," Proceedings of the 10-th Int. Conf. HoloExpo-2013, 257-264 (2013) [in Russian].
2. I. E. Golub, A. N. Malov, A. V. Neupokoyeva, and L. V. Sorokina, "Registration of laser-induced microstructure changes of blood plasma by the wavelet analysis of speckle patterns," Proceedings of V Troitsk Conference Medical Physics and Innovations in Medicine 1, 252-254 (2012) [in Russian].
3. M. A. Vilenskii, D. N. Agafonov, D. A. Zimnyakov, V. V. Tuchin, and R. A. Zdrazhevskii, "Speckle-correlation analysis of the microcapillary blood circulation in nail bed," Quantum Electron. 41(4), 324–328 (2011).
4. I. V. Fedosov, and V. V. Tuchin, "The space-time correlation of the intensity of a speckle field formed as a result of scattering of focused coherent radiation by a capillary liquid flow containing scattering particles," Opt. Spectrosc. 93(3), 434–438 (2002).
5. A. N. Malov, E. S. Musatova, A. U. Setejkin, and S. V. Zinoviev "Laser nanoclasterization processes simulation," Proceedings of the 8th Russia and China Pharmaceutical Forum Modern Problems of Nanopharmacology, 66 – 67 (2011).
6. V. N. Shabalin, and S. N. Shatokhina, Morphologies of Human Biological Liquids, Khrizostom, Moscow (2001) [in Russian].
7. A. N. Malov, E. S. Musatova, and A. Y. Seteikin, "Crystallographic registration of the results of laser nanocrystallisation of bioorganic liquids," Proceedings of V Troitsk Conference Medical Physics and Innovations in Medicine 2, 80-82 (2012) [in Russian].
8. R. Paringer, A. Kupriyanov, and N. Ilyasova, "Dendritic crystallogram images classification," JBPE 1(2), 135–138 (2015).
9. N. Y. Ilyasova, A. V. Kupriyanov, and A. G. Khramov, Information Technologies of Image Analysis in the Problems of Medical Diagnostics, Radio i svyaz, Moscow, (2012) [in Russian].
10. Y. Y. Tarasevich, "Mechanisms and models of the dehydration self-organization in biological fluids," Phys.-Usp. 47(7), 717–728 (2004).
11. A. N. Malov, A. Y. Seteikin, A. V. Neupokoeva, E. S. Musatova, I. E. Golub, L. V. Sorokina, and A. A. Vaichas, "The laser radiation action on the biological objects," Optik - International Journal for Light and Electron Optics 124(23), 6034–6041 (2013).
12. J. S. Bendat, and A. G. Piersol, Engineering Applications of Correlation and Spectral Analysis, John Wiley&Sons, New York (1980). ISBN: 978-0471570554.

1 Introduction

In the monitoring of laser impact on multicomponent or hardly standardisable media (protein solutions, blood plasma, petrol, gelatine-based holographic media) the possibility of fast obtaining the processing results could significantly increase the efficiency of the impact, or could allow the choice of the impact parameters corresponding to the specific features of the particular medium [1-4]. For such media, represented by the solutions of complex organic molecules, a few methods were proposed to determine the structure inhomogeneities.

One of the simplest and clear methods for monitoring the structure modifications in liquid media is crystallography, in which the segment size of a crystallogram is directly related to the characteristic size of inhomogeneities in biological liquids [5-9].

The phenomenon of dehydration self-organisation is chosen to be the basis of one of the medical diagnostic methods, the method of wedge-shaped dehydration [8-10] that consists in the following. A droplet of the studied biological liquid (for the control samples and the ones exposed to laser radiation) with the volume 0.01 ml is deposited on the defatted object glass and dried tilted at the angle 25-30º and dust-protected at room temperature 20-25ºC and relative air humidity 65-70% during 18-24 hours. Using this method the crystallograms of the preparations of the studied biological liquids were obtained. The drawback of this method is the impossibility of controlling the liquid structure in real time, since the preparation (drying) of a crystallogram takes a few hours.

In Ref. [7] it was shown that the size of the crystals essentially changes under the exposure of the glycine solution with the concentration 5% to the radiation of a red helium-neon laser with the wavelength 633 nm during 15 min, the radiation power density being nearly 0.6 mW/cm^2 (Fig. 1). Thus, when the crystallograms are formed in dry films from 5% solution of glycine, their structure is determined by the nucleation centres, which, in turn, depend upon the state of the initial solution. The bioorganic molecules in a solution have the aqueous environment and form clusters with different size and configuration. When the solution is dried, the large-size clusters having smaller velocity of chaotic motion are first of all fixed at the substrate and play the role of nucleation centres for the growth of crystals in the film.

Then the epitaxial growth of the film occurs at the expense of the later crystallised low-molecular fractions fixed on the dendrite-like base. In this way a ray-shaped pattern of lamellas with epitaxial recrystallization on the ray part playing the role of the substrate for the ex-siccant solution is formed. The reduction of the thickness of the lamella rays after the laser irradiation shows that in the irradiated solution the cluster size is considerably reduced, which leads to the size reduction of the nucleation centres in the course of the film drying [5, 7, 11].

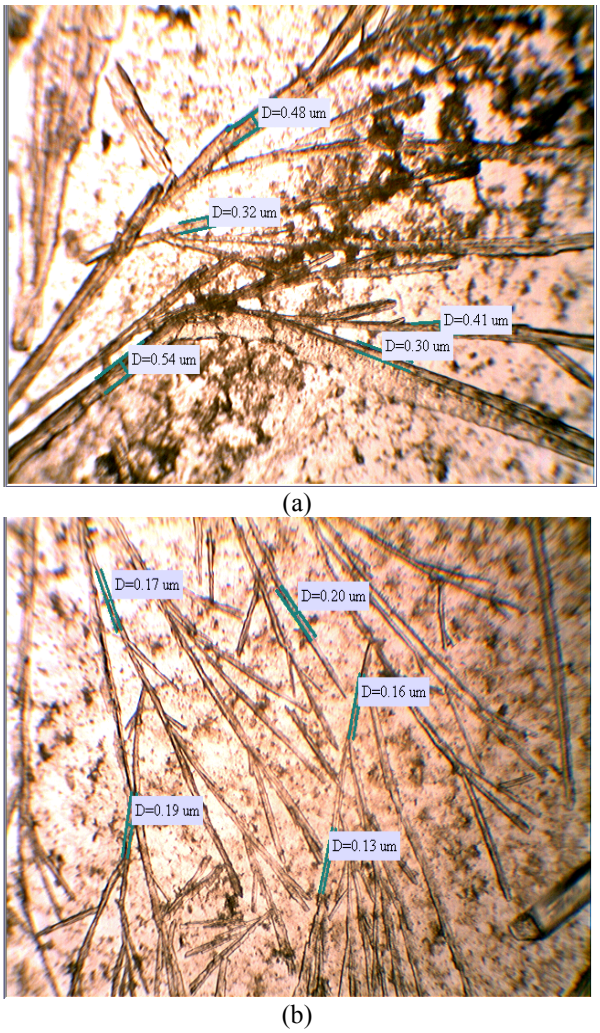


Fig. 1 5% glycine solution under the 50× magnification. (a) the control sample; (b) after laser treatment system.

An alternative method of structure monitoring is to use the speckle pattern of the studied liquid. Since the size of the organic molecular associates, e.g., of those having the protein nature, can by many times exceed the size of an individual molecule, such complexes will manifest themselves as essential fluctuations of the refractive index in the solution and will be the objects at which the diffraction of the laser radiation occurs. Speckle patterns are formed as a result of interaction of coherent laser radiation with nonuniformity medium. According to the diffraction laws, the characteristic spot size of the speckle pattern is inversely proportional to the inhomogeneity size. At present the speckle optical methods of diagnostics of liquids, biological objects, and solid surfaces are intensely developed, since the speckle patterns contain a large amount of information about the size, concentration, and motion velocities of in-homogeneities within the bulk sample.

On the other hand, there is an urgent issue of selecting the useful information contained in speckle patterns from the random components related to the presence of multiple optical surfaces, parasitic illumination, etc., in the optical schemes. Thus, the aim

of the present paper is to elaborate an algorithm for processing speckle patterns and crystallograms, as well as to introduce numerical criteria that would allow the efficient comparison of images, obtained at different stages of monitoring.

2 Materials and Methods

In the present work the object of study including the formation of crystallograms was the Grippferon solution, the main component of which is interferon alpha-2b, the protein-nature factor that provides antivirus immunity. The Grippferon solution in a cuvette was subjected to the laser radiation (the mean wavelength 655 nm, the intensity about 80 mW/cm^2) during 20 minutes. Then the irradiated and the control solution was poured on similar glass substrates and kept at room temperature for obtaining the crystallograms. The series consisted of ten similar experiments, in which similar-type crystallograms were obtained for the appropriate time of exposure.

The speckle patterns were obtained from the gelatine solution in the gelling process of its. For this goal the spatial distribution of laser radiation after passing through the cuvette with gelatine solution was recorded by means of a digital photo camera. The gelatine solution with the concentration 10% (by the mass of dry gelatine) kept in the water bath at the temperature 50°C, was placed in a cuvette near the focus of the laser beam (Fig. 2). The scattered radiation was recorded immediately after the installation of the solution into the setup (the beginning of gelling) and then each 5 minutes until the final time of 30 minutes, during which the solution turned into gel.

The wavelength of the probe radiation was 655 nm, the intensity was about 150 mW/cm^2. The preparation of the gelatine solution, the process of gelling, and the recording of speckle patterns was repeated 5 times under the similar conditions. The dynamics of the numerical parameters of the speckle patterns was similar in all experiments.

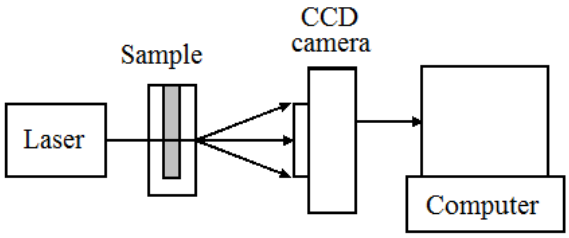


Fig. 2 Schematic diagram of the experimental setup.

The resulting speckle patterns were used to calculate the autocorrelation coefficient. The correlation is known to be expressed by the convolution integral, where the functions $g(x)$ and $h(x)$ correspond to the intensity distribution functions in the studied patterns:

$$K(x,y)=\iint g(\xi,\eta)\cdot h(x-\xi,y-\eta)\,d\xi\,d\eta=F^{-1}\{G(\xi,\eta)\cdot H(\xi,\eta)\}.$$

For the autocorrelation function we have

$$A(x,y)=\iint g(\xi,\eta)\cdot g(x-\xi,y-\eta)\,d\xi\,d\eta=F^{-1}\{G(\xi,\eta)\cdot G(\xi,\eta)\}.$$

For the calculations we used the convolution theorem, i.e., at first the Fourier transform was calculated for each pattern using the FFT algorithm, then the Fourier transforms were multi-plied, and then the inverse Fourier transform was calculated. The resulting autocorrelation function is a function of two coordinates $A(x,y)$. Numerically this is a matrix, the dimension of which depends on the initial size of the speckle pattern. The graphic representation of this matrix looks like a pyramid, the surface of which depends upon the properties of the studied pattern (Fig. 3). For convenience we took square speckle patterns, and therefore, the coefficients of autocorrelation were represented by square matrices.

In the vicinity of zero a certain peak is observed, the width of which can be estimated at some level, e.g., 0.9 or 1/e of the maximum. The advantage of this method is that the data of the entire speckle pattern are taken into account, and the drawback is the dependence of the autocorrelation coefficient upon the brightness of the speckle pattern, which can make the interpretation difficult, as well as the loss of data on the structure of the autocorrelation pyramid, if only the central peak width is used as a numerical parameter.

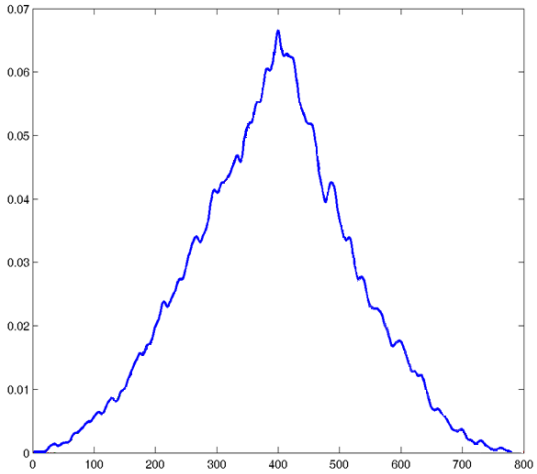


Fig. 3 Typical view of the autocorrelation function in the diagonal section.

The real autocorrelation function (Fig. 3) has complex shape that makes the determination of its half-width difficult. The local oscillations of the function are due to the fact that the speckle pattern at finite sampling can be considered as a quasiperiodic function, which gives rise to the oscillations. To estimate the correlation radius, one can take the separation between the peak

centre and the nearest local maximum (this distance corresponds to the mean size of a speckle). The error of such method can be estimated as 7- 10% [12].

As an alternative method of speckle pattern processing we used the algorithm based on the binarisation of the obtained image. This method was also used to derive numerical estimates from the crystallograms.

The image processing program was written basing on the library OpenCV (Open Source Computer Vision Library), a computer vision library with open source code. In medicine OpenCV is used in the processing of X-ray/MRT/CT images. For the processing of crystallograms in the official documentation of the OpenCV library, we used the algorithm of contour processing. The procedure includes the image binarisation according to the chosen level. All pixels with the brightness above this level are considered white, and all other pixels are considered black. Then the mean width and height of the obtained spots and their mean area are calculated. The resulting data (images with contour boundaries, numerical characteristics) are written in a file and displayed on the screen. We also added the possibility of filtering small contours (in the final image they are shown in a different colour and are not taken into account in calculations) [11].

3 Experimental results

The typical crystallogram view and the results of processing are presented in Fig. 4. The pattern binarisation level was chosen similar in all cases to provide the comparability of the patterns in the series and amounted to 130% of the mean brightness of the pattern, calculated in the program. Lighter contours are those not taken into account in the calculations. The threshold contour size below which a contour was excluded from the general statistics was chosen 10% of the current mean size. For example, if the program returned the mean contour size of 40 pixels, then the contours smaller than 4 pixels were neglected. The results of the calculations are presented in Fig. 5. Before the laser impact the mean speckle size was X=57.6 pixels by Y=61.2 pixels. After the impact the mean pixel size appeared to be X=38.6 pixels by Y=45.3 pixels. One pixel of the image corresponds to the inhomogeneity of about 30 μm.

The program calculating the mean contour size was also used to analyse the speckle pat-terns (Fig. 6). The results of the processing of the speckle patterns recorded at different moments of time starting from the beginning of the gelling process are presented in Fig. 7.

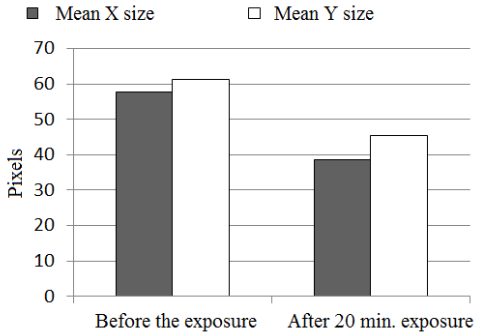


Fig. 5 Change of the characteristic pattern scale, obtained using the computer processing.

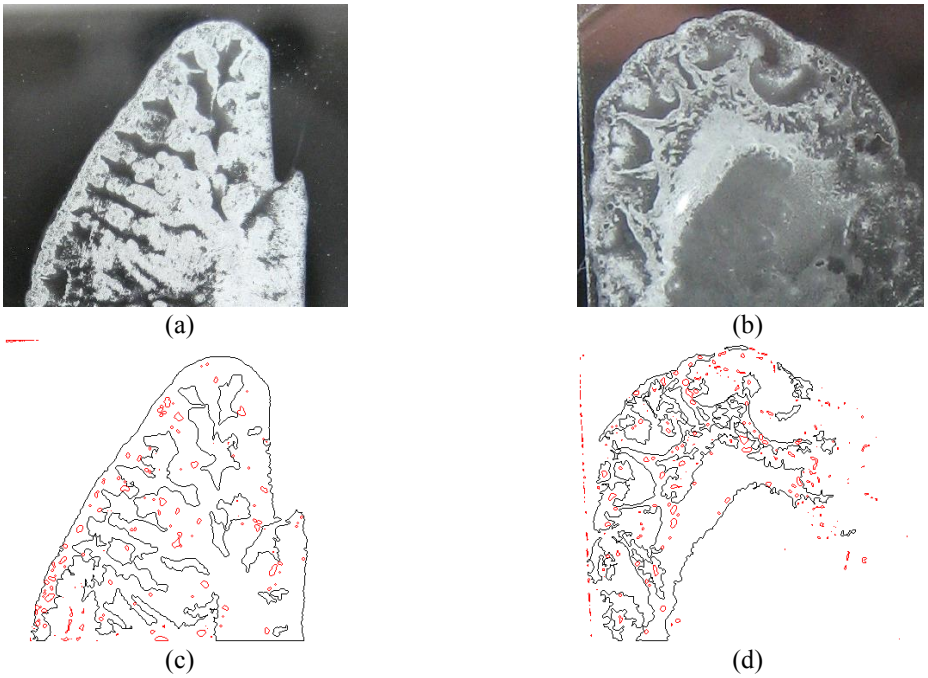
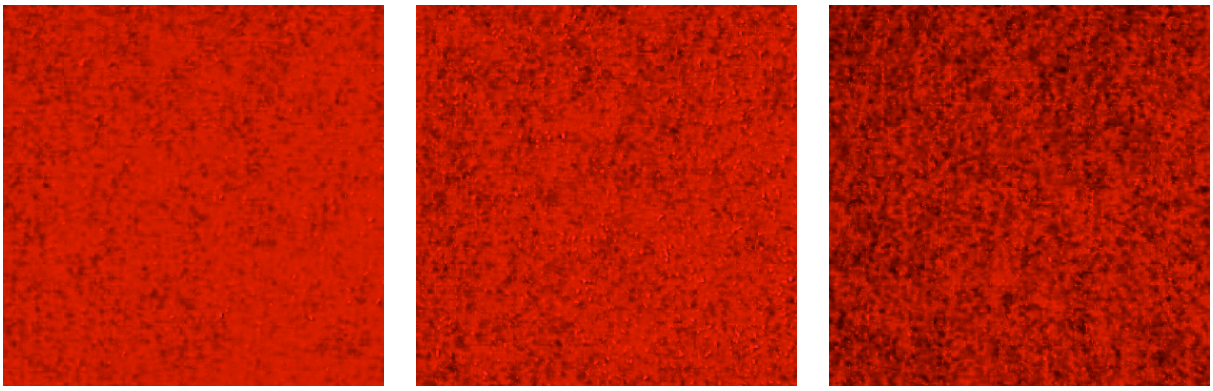


Fig. 4 View of the solution crystallogram without the laser radiation impact (a) and after the 20 minutes of exposure (b), as well as the respective crystallograms after the contour selection (c), (d).



(a) (b) ©

Fig. 6 Speckle patterns recorded in the course of the gelatine gelling: (a) - immediately after placing the solution into the recording system (gelling just started); (b) - 10 minutes later; (c) - 20 minutes after the beginning of the gelling process.

One can see that at small gelling times (up to 10 minutes) the speckle size decreases, which is due to the unfolding of the gelatine secondary structures. Then the structure evolves into more compact aggregates. Finally, at large times of gelling (more than 20 minutes) the speckle size sharply decreases, which is a fingerprint of the formation of large-scale spatial structures over the entire volume of the solution.

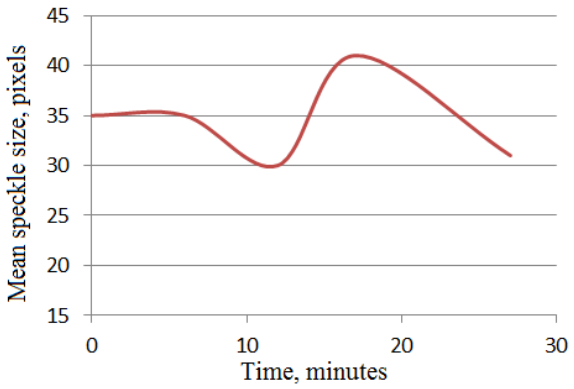


Fig. 6 Dynamics of mean speckle area versus the time of gelatine gelling, calculated using the program OpenCV.

4 Conclusion

The proposed method of contour selection and calculating the mean contour size allows the introduction of the quantitative characteristic for comparing the crystallograms from liquids under the different external conditions or at different stages of the study. The algorithm described in the paper can be also applied to develop a numerical criterion for comparing the speckle patterns from different samples of the studied liquid. The advantages of the proposed image processing technique are its high sensitivity, small processing time and clearness of results.

Choosing the probe radiation wavelengths for noninvasive monitoring of haemoglobin in blood

Igor L. Davydkin[1], Natalia S. Kozlova[1*], Vadim N. Koniukhov[2], Tatiana P. Kuzmina[1], and Elizaveta V. Mordvinova[1]

[1] Samara State Medical University, 89 Chapaevskaya str., Samara 443099, Russia
[2] Samara State Aerospace University, 34 Moskovskoe shosse, Samara 443086, Russia

[*] **e-mail:** gorachaia@live.ru

Abstract. The goal of our study was to estimate the accuracy of measuring the blood haemoglobin concentration by means of the pulse CO-oximetry, depending on the probe radiation wavelength.
Revealing the combinations of wavelengths, optimal for minimising the measurement error, will allow the formulation of requirements to the instruments for noninvasive assessment of haemoglobin concentration, applicable in wide clinical practice. To solve this problem, we examined a group of haematological patients in the Haematology Department of the Samara State Medical University Clinic with the aim to compare the results obtained using the experimental multiwave system for noninvasive haemoglobin concentration assessment and the results of the clinical blood analysis. © 2016 Journal of Biomedical Photonics & Engineering.

Keywords: monitoring, hemoglobin, noninvasive diagnosis, laser.

Paper #2835 received 2015.12.23; revised manuscript received 2016.03.10; accepted for publication 2016.03.10; published online 2016.03.31. doi: 10.18287/JBPE16.02.010305

References

1. J. W. McMurdy, G. D. Jay, S. Suner, and G. Crawford, "Noninvasive Optical, Electrical, and Acoustic Methods of Total Hemoglobin Determination," Clinical Chemistry 54(2), 264-272 (2008).
2. K. Saigo, S. Imoto, M. Hashimoto, H. Mito, J. Moriya, T. Chinzei, Y. Kubota, S. Numada, T. Ozawa, and S. Kumagai, "Noninvasive Monitoring of Hemoglobin: The Effects of WBC Counts on Measurement," Am. J. Clin. Pathol. 121(1), 51-55 (2004).
3. E. V. Kozhokina, "Noninvasive methods of measuring bilirubin, haemoglobin, and glucose. The haemobiliglucometer instrument," Scientific and Technical Journal of Information Technologies, Mechanics and Optics 2(72), 157-162 (2011). [in Russian].
4. R. Kumar, and H. Ranganathan, "Noninvasive Sensor Technology for Total Hemoglobin Measurement in Blood," Journal of Industrial and Intelligent Information 1(4), 243-246 (2013).
5. R. Doshi, and A. Panditrao, "Non-Invasive Optical Sensor for Hemoglobin Determination," International Journal of Engineering Research and Applications 3(2), 559-562 (2013).
6. J. E. Bender, A. B. Shang, E. W. Moretti, B. Yu, L. M. Richards, and N. Ramanujam, "Noninvasive monitoring of tissue hemoglobinusing UV-VIS diffuse reflectance spectroscopy: a pilot study," Optics Express 17(26), 23396-23409 (2009).
7. U. Timm, G. Leen, E. Lewis, D. McGrath, J. Kraitl, and H. Ewald, "Non-Invasive Optical Real-time Measurement of Total Hemoglobin Content," Procedia Engineering 5, 488-491 (2010).
8. D. J. Deyo, R. O. Esenaliev, O. Hartrumpf, M. Motamedi, and D. S. Prough, "Continuous noninvasive optoacoustic monitoring of hemoglobin concentration," Anesthesiol Analgesia 92(S139), (2001).
9. I. Y. Petrova, R. O. Esenaliev, Y. Y. Petrov, H. P. E. Brecht, C. H. Svensen, J. Olsson, D. J. Deyo, and D. S. Prough, "Optoacoustic monitoring of blood hemoglobin concentration: a pilot clinical study," Opt. Lett. 30(13), 1677–1679 (2005).
10. G. Lindner, and A. K. Exadaktylos, "How Noninvasive Haemoglobin Measurement with Pulse CO-Oximetry Can Change Your Practice: An Expert Review," Emerg. Med. Int. 2013, 701529 (2013).

11. D. Frasca, C. Dahyot-Fizelier, K. Catherine, Q. Levrat, B. Debaene, and O. Mimoz, "Accuracy of a Continuous Noninvasive Hemoglobin Monitor in Intensive Care Unit Patients," Crit. Care Med. 39(10), 2277-2282 (2011).
12. Rad-57. Signal Extraction Pulse CO-Oximeter, Operator's manual (2011).
13. Radical-7. Signal Extraction Pulse CO-Oximeter, Operator's manual (2010).
14. S. Prahl, "Optical absorption of hemoglobin," Oregon Medical Laser Center (1999).
15. O. Siggaard-Andersen, B. Norgaard-Pedersen, and J. Rem, "Hemoglobin pigments spectrophotometric determination of oxy-, carboxy-, met-, and sulfhemoglobin in capillary blood," Clinica Chimica Acta 42(1), 85-100 (1972).
16. L. Randeberg, J. Bonesronning, M. Dalaker, J. Nelson, and L. Svaasand, "Methemoglobin formation during laser induced photothermolysis of vascular skin lesions," Lasers in Surgery and Medicine 34(5), 414-419 (2004).
17. M. Meinke, G. Müller, M. Friebel, and J. Helfmann, "Optical properties of platelets and blood plasma and their influence on the optical behavior of whole blood in the visible to near infrared wavelength range," J. Biomed. Opt. 12(1), 014024 (2007).
18. R. M. Pope, and E. S. Fry, Absorption spectrum (380-700 nm) of pure water. II. Integrating cavity measurements, Applied Optics 36(33), 8710-8723 (1997).
19. K. F. Palmer, and D. Williams, "Optical properties of water in the near infrared," Journal of the Optical Society of America 64(8), 1107-1110 (1974).
20. J. Coquin, A. Dewitte, Y. L. Manach, M. Caujolle, O. Joannes-Boyau, C. Fleureau, G. Janvier, and A. Ouattara, "Precision of noninvasive hemoglobin-level measurement by pulse co-oximetry in patients admitted to intensive care units for severe gastrointestinal bleeds," Critical Care Medicine 40(9), 2576-2582 (2012).
21. L. J. Moore, C. E. Wade, L. Vincent, J. Podbielski, E. Camp, D. Junco, H. Radhakrishnan, J. McCarthy, B. Gill, and J. B. Holcomb, "Evaluation of noninvasive hemoglobin measurements in trauma patients," The American Journal of Surgery 206(6), 1041-1047 (2013).

1 Introduction

The main advantages of noninvasive methods for the analysis of blood protein components are the removal of the infection risk, the efficiency, the possibility of continuous monitoring, the absence of biologic pollution, and the softened requirements to the personnel qualification. Various methods [1-9] can be used to assess the blood haemoglobin concentration in vivo.

Among these methods, the optical ones are most acceptable for the practical use. This is due to the relative simplicity of the instrumentation required to implement the optical methods of noninvasive haemoglobin concentration and the techniques for clinical applications. The analysis of trends in the development of optical methods and technical means for assessment of haemoglobin concentration shows that the main trend lies in the field of using the method of pulse CO-oximetry [10, 11].

The method of pulse CO-oximetry is based on measuring the optical radiation attenuation by the arterial blood at different wavelengths and calculating the concentrations of the total haemoglobin and its fractions from the obtained attenuation values. The number of probe wavelengths determines the number of determined fractions of haemoglobin. Thus, in the commercially produced monitors Rad-57 and Raical-7 (Masimo) twelve wavelengths are used [12, 13] and the concentrations of the total haemoglobin, oxyhaemoglobin, carboxyhaemoglobin, and methaemoglobin are determined. However, in many practical cases, e.g., for the anaemia diagnostics, the information on the fractional composition is abundant, and it is sufficient to know the total haemoglobin concentration solely. In this relation, the question arises about the set of probe radiation wavelengths necessary to determine the blood haemoglobin concentration with acceptable accuracy.

The aim of our study was to estimate the accuracy of measuring the blood haemoglobin concentration by means of the pulse CO-oximetry method depending on the chosen wavelengths of the probe radiation. The determination of the set of wavelengths minimising the measurement error will offer an opportunity to optimise the construction of the instrument for noninvasive assessment of the haemoglobin concentration from the point of view of scheme simplification and, therefore, cost reduction. In turn, the cost reduction and device simplification will allow the implementation of this method in wide clinical practice of the population screening, aimed at revealing the persons with diseases that affect the haemoglobin concentration.

To solve the formulated problem the studies were carried out with the aim of comparing the results obtained using the experimental multiwave system for noninvasive assessment of the blood haemoglobin concentration and the data of clinical blood analysis. The essence of the study was to determine the measurement error for different linear combinations of wavelengths. The experimental examinations were carried out in the group of haematological patients with different pathologies on the base of the Haematology Department of Samara State Medical University.

2 Theoretical foundation of the pulse CO-oximetry

The method of pulse CO-oximetry is based on the Bouguer-Lambert-Beer law that relates the reduction of the intensity of light that passes through a layer of light-absorbing matter to the concentration of the absorbing substance and the layer thickness:

$$I = I_0 \cdot 10^{-\varepsilon \cdot l \cdot c}, \quad (1)$$

where ε is the molar absorption coefficient, l is the thickness of light-absorbing layer (m), c is the concentration of the stained solution (M). For several stained substances present in the solution the contributions are additive, i.e., $A = A_1 + A_2 + \ldots + A_n$, where A is the total optical density of the solution defined as $-\lg T = A = \varepsilon \cdot l \cdot c$, where $\boldsymbol{T = \frac{I}{I_0}}$.

We assume that the optical path lengths are similar for the optical radiation with difference wavelengths propagating through the sample and that the Bouguer-Lambert-Beer law is valid. Then to determine the concentration of each of n stained substances one has to solve the system of linear equations

$$\begin{cases} \mathrm{A}\ (\lambda_1) = \varepsilon_1(\lambda_1)\cdot C_1 + \varepsilon_2(\lambda_1)\cdot C_2 + \ldots + \varepsilon_n(\lambda_1)\cdot C_n \\ \mathrm{A}\ (\lambda_2) = \varepsilon_1(\lambda_2)\cdot C_1 + \varepsilon_2(\lambda_2)\cdot C_2 + \ldots + \varepsilon_n(\lambda_2)\cdot C_n \\ \ldots\ldots\ldots\ldots\ldots\ldots\ldots\ldots\ldots\ldots\ldots\ldots\ldots\ldots\ldots\ldots \\ \mathrm{A}\ (\lambda_n) = \varepsilon_1(\lambda_n)\cdot C_1 + \varepsilon_2(\lambda_n)\cdot C_2 + \ldots + \varepsilon_n(\lambda_n)\cdot C_n \end{cases}, \quad (2)$$

To estimate the amount of haemoglobin ($\boldsymbol{C_{HbTotal}}$), one has to determine the mass of all haemoglobin fractions and the volume of plasma, in which they are dissolved. The direct measurement of these parameters by means of spectrophotometry is impossible, but one can determine the concentration of fractions and then, by plotting the regression dependences found from the blood clinical analysis, estimate the amount of blood haemoglobin.

The main fractions of blood haemoglobin are oxyhaemoglobin ($\boldsymbol{C_{HbO_2}}$), deoxyhaemoglobin ($\boldsymbol{C_{Hb}}$), carboxyhaemoglobin ($\boldsymbol{C_{HbCO_2}}$), and methaemoglobin ($\boldsymbol{C_{HbMet}}$). Normal blood mainly contains $\boldsymbol{C_{HbO_2}}$ and $\boldsymbol{C_{Hb}}$, while the part of dysfunctional fractions ($\boldsymbol{C_{HbCO_2}}$, $\boldsymbol{C_{HbMet}}$) does not exceed 3%. Besides, in the norm the fraction of $\boldsymbol{C_{HbO_2}}$ amounts to nearly 98%. Therefore, the first rough approximation the optical medium can be presented as double-layered, consisting of oxyhaemoglobin and blood plasma. Since the blood plasma consists of 90% water, the set of equations (2) will take the form

$$\begin{cases} \mathrm{A}\ (\lambda_1) = \varepsilon_{HbO2}(\lambda_1)\cdot C_{HbO2} + \varepsilon_{H2O}(\lambda_1)\cdot C_{H2O} \\ \mathrm{A}\ (\lambda_2) = \varepsilon_{HbO2}(\lambda_2)\cdot C_{HbO2} + \varepsilon_{H2O}\ (\lambda_2)\cdot C_{H2O} \end{cases}, \quad (3)$$

and therefore,

$$C_{HbO2} = \frac{\varepsilon_{H2O}(\lambda_2)\cdot \mathrm{A}\ (\lambda_1) - \varepsilon_{H2O}(\lambda_1)\cdot \mathrm{A}\ (\lambda_2)}{\varepsilon_{HbO2}(\lambda_1)\cdot\varepsilon_{H2O}(\lambda_2) - \varepsilon_{HbO2}(\lambda_2)\cdot\varepsilon_{H2O}(\lambda_1)},$$

$$C_{H2O} = \frac{\varepsilon_{HbO2}(\lambda_1)\cdot \mathrm{A}\ (\lambda_2) - \varepsilon_{HbO2}(\lambda_2)\cdot \mathrm{A}\ (\lambda_1)}{\varepsilon_{HbO2}(\lambda_1)\cdot\varepsilon_{H2O}(\lambda_2) - \varepsilon_{HbO2}(\lambda_2)\cdot\varepsilon_{H2O}(\lambda_1)}. \quad (4)$$

The analysis of Eqs. (3) shows that to increase the sensitivity and to reduce the error one has to choose the wavelengths providing a large difference between the absorption coefficients of two different components. The optimal choice of wavelengths is of particular importance when using the pulse CO-oximetry method, in which the measured quantity is the increment of absorption due to the systolic increase of blood volume rather than the absolute absorption. This increment depends upon the haemodynamic specific features of the arterial vessels in the limbs of a particular person, the current functional state, and the conditions of measurement. Usually this increment does not exceed 5-7%, the mean value being 1%, and in the case of haemodynamic pathology it can be as small as a few tenths of per cent.

With the absorption spectra of the main haemoglobin fractions, blood plasma, and water in the visible and near-infrared ranges [14-19] taken into account, the probe wavelengths for the experimental studies were chosen as 520 nm, 658 nm, 776 nm, 839 nm, 974 nm, 1348 nm, and 1550 nm. The choice was justified by the fact that at 520 nm, 658 nm, 776 nm, 839 nm, and 974 nm the absorption coefficient for different forms of haemoglobin by an order of magnitude or more exceeds that of water. On the contrary, at the wavelengths 1348 nm and 1550 nm the absorption by water is essentially greater than the absorption by the haemoglobin fractions.

3 Experimental system and processing algorithms for noninvasive assessment of haemoglobin concentration

The system for noninvasive assessment of blood haemoglobin concentration was developed at the Chair of Laser and Biotechnical Systems of Samara State Aerospace University. The system consists of the electronic-optical registration unit and the special software operating under OS Windows. The registration unit incorporates the electronic circuit connected to the optical finger sensor via the optical fibre line. In the registration unit the semiconductor lasers radiating at the wavelengths 520, 658, 776, 839, 974, 1348, and 1550 nm are mounted.

The electric power supply of the laser units and the stabilisation of their temperature are implemented by means of the control circuits that switch the lasers on sequentially and provide the constant pulse power and wavelength of radiation. Through the optical fibre cable, the laser radiation is delivered to the biological object and after passing through it is detected by the broadband InGaAs photodiode. The photocurrent output from the

photodiode, proportional to the attenuation of the radiation by the biological tissues, arrives at the amplifier and then at the synchronous demodulator, in which the multiplexing and the formation of the signals of the attenuation spectral components occurs. These signals, containing constant and variable components, are digitised by the multichannel delta-sigma ADC and are transmitted via the USB to the personal computer for further processing.

Generally, the algorithms of processing the radiation attenuation signals included the following basic stages: the detection of pulse waves, the estimation of the pulse wave amplitude at each wavelength, the estimation of haemoglobin concentration. The detection of pulse waves was implemented by comparison with the filtered signal threshold. The comparison threshold was chosen as a part of the filtered signal amplitude and was dynamically varied with the variation of the signal depending on the registration conditions. The signal filtering was implemented using a bandpass filter formed by a superposition of high-pass and low-pass filter. The filtering was implemented by averaging the photoplethysmographic signal over all channels for low frequencies and by the signal differentiation for high frequencies. The time constant of the differentiator was chosen to maximise the signal-to-noise ratio.

The signal amplitude was calculated using the maximum likelihood estimate

$$\hat{A} = \frac{\int_0^T X(t)S_1(t)dt}{\int_0^T S_1^2(t)dt}, \quad (5)$$

where $X(t)$ is the current signal in the channel, $S_1(t)$ is the reference signal, [0, T] is the duration of a single pulse wave. The rectangular signals with different durations and the signal obtained by averaging the pulse wave realisations were used as reference signals. The obtained estimates of amplitudes were analysed for the presence of outliers and filtered using either the sigma clipping algorithm, or the median filter.

After the determination of the sequence of algorithms for the primary processing of signals, optimal from the point of view of the error variance minimisation, the data were used for the estimation of haemoglobin concentration.

To estimate the haemoglobin concentration we used the multifactor linear regression model, implemented using the MATLAB application software. The factors for the regression model were the normalised ratios of radiation attenuations at different wavelengths. These ratios were calculated as

$$R_{\lambda_i/\lambda_j} = \frac{\Delta A(\lambda_i)/A(\lambda_i)}{\Delta A(\lambda_j)/A(\lambda_j)}, \quad (6)$$

where $\boldsymbol{A(\lambda_{i,j})}$ is the constant component and $\boldsymbol{\Delta A(\lambda_{i,j})}$ is the variable component of the attenuation of optical radiation at the i-th and j-th wavelength, respectively. We could not calculate the factors for the wavelengths 520 and 1550 nm because of strong attenuation of the signal at these wavelengths and, consequently, the low signal-to-noise ratio. Thus, 8 linearly independent factors were formed, namely $\boldsymbol{R_1 = R_{\lambda_1/\lambda_5}}$, $\boldsymbol{R_2 = R_{\lambda_2/\lambda_5}}$, $\boldsymbol{R_3 = R_{\lambda_3/\lambda_5}}$, $\boldsymbol{R_4 = R_{\lambda_4/\lambda_5}}$, $\boldsymbol{R_5 = R_{\lambda_1/\lambda_4}}$, $\boldsymbol{R_6 = R_{\lambda_2/\lambda_4}}$, $\boldsymbol{R_7 = R_{\lambda_3/\lambda_4}}$, $\boldsymbol{R_8 = R_{\lambda_2/\lambda_3}}$, where $\boldsymbol{\lambda_1}$ =658 nm, $\boldsymbol{\lambda_2}$ =776 nm, $\boldsymbol{\lambda_3}$=839 nm, $\boldsymbol{\lambda_4}$ = 974 nm, and $\boldsymbol{\lambda_5}$=1348 nm. With these factors the linear model was constructed:

$$SHb = a_0 + a_1R_1 + a_2R_2 + a_3R_3 + a_4R_4 + a_5R_5 + a_6R_6 + a_7R_7 + a_8R_8 \quad (7)$$

where SHb is the haemoglobin concentration estimate, $a_0 \ldots a_8$ are the linear model coefficients, determined from the data of clinical analysis.

4 Results of experimental studies

The studies were carried out at the Chair of Haematology of Samara State Medical University. The measurements of haemoglobin concentration using the laboratory method ( ) were performed in the group of 90 patients with different pathologies of haematological profile. The range of variation of the haemoglobin concentration in the studied group amounted to 47-190 g/L, and the haematocrit varied within 15-61 %. Then in the same patients during 30 seconds the multiwave photoplethysmogram was recorded and processed using the above algorithm. The regression model factors were calculated using Eq. (5). Thus, the data matrix was completed in the form

$$\begin{pmatrix} R_{11}, R_{12}, R_{13}, R_{14}, R_{15,} R_{16}, R_{17,} R_{18,} LHb_1 \\ \ldots\ldots\ldots\ldots\ldots\ldots\ldots\ldots\ldots\ldots \\ R_{n1}, R_{n2}, R_{n3}, R_{n4}, R_{n5,} R_{n6}, R_{n7,} R_{n8,} LHb_n \end{pmatrix} \quad (8)$$

where n=90.

Then using 50 randomly chosen lines of the matrix (8) the coefficients for the regression model (7) were calculated and for all patients the values of SHb were determined. The results obtained using the system were compared with the results of the blood clinical analysis. The statistics of the difference SHb – LHb was calculated. In the case of using all 8 factors in the model (6) the root-mean-square deviation $\boldsymbol{\sigma}$ =20.45 g/l. the mathematical expectation $\boldsymbol{m}$ =0, the $\boldsymbol{median}$ = −2.3. The histogram of the differences SHb – LHb for this case is presented in Fig. 1.

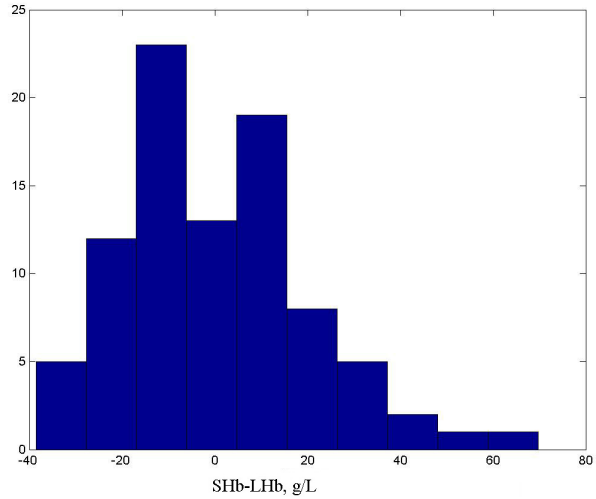


Fig. 1 Histogram for the differences *SHb – LHb* in the case of using 8 factors.

After that, some factors were excluded from the model (6) to determine such combination of factors, for which the root-mean-square is minimal in the case of using a smaller number of probe wavelengths. It was found that this is achieved with the factors R_1, R_2, R_4. In this case the root-mean-square deviation $\boldsymbol{\sigma}$ =21.0 g/l, the mathematical expectation $\mathbf{m} = \mathbf{0}$, the $\mathbf{median} = -1.8$. The histogram of differences SHb – LHb for this case is presented in Fig. 2. In this case the mathematical expectation can be considered as the systematic error of the measurement, and the root-mean-square deviation as the random error.

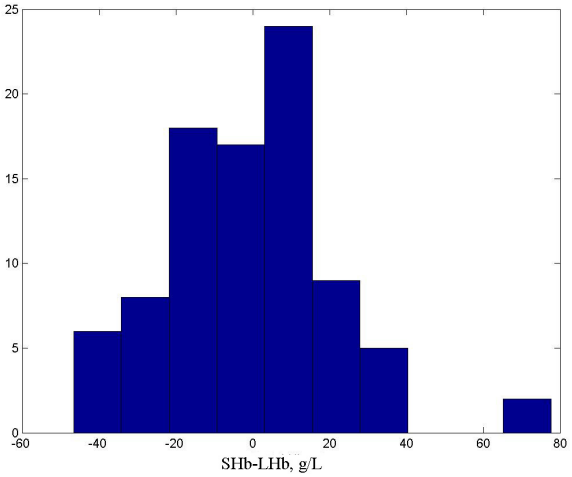


Fig. 2 Histogram for the differences *SHb – LHb* in the case of using the factors R_1, R_2, R_4.

The studies have shown that the exclusion of $\boldsymbol{\lambda_3} = 839$ nm from the set of probe wavelengths insignificantly increases the root-mean-square deviation, while the mathematical expectation is not changed at all.

The attempt to compare the obtained results with those of the noninvasive haemoglobin measurements carried out using the commercial monitors Raical-7 and Rad-87 (Masimo) in different clinical investigations shows the following. The data on the measurement accuracy, defined as the root-mean-square deviation *SHb – LHb* strongly differ in different sources and are hardly comparable. Thus, in the review [10] for different cases the mathematical expectation varies within the range from 0 to 8 g/L, and the root-mean-square deviation from 5 to 13 g/L. However, in Ref. [20] $\boldsymbol{m} = 10$ g/l, and $\boldsymbol{\sigma} = 19$ g/l. The difficulty of comparing these data is related to the difference in ranges of haemoglobin variation in the groups of patients of different age and sex, the lack of data on the quality of the recorded signals of arterial blood pulsation, on whether the outlier rejection was performed or not, the diversity of pathologies, etc.

Another approach to the assessment of noninvasive haemoglobin measurement precision is presented in Ref. [21]. In this paper the authors determine the 95% confidence interval for the difference *SHb – LHb*. It was found that for the measurement of haemoglobin in the interval from 80 to 170 g/L the 95% confidence interval amounts to 71.8 g/L.

We carried out the analogous studies and found that in the case of using 8 factors the 95% confidence interval, obtained by means of our experimental multiwave system appeared to be 73.2 g/L, and with three factors R_1, R_2, R_4 it was 80.7 g/L, which is worse. However, the range of variation for the haemoglobin concentration in our group was 47-190 g/L, which is larger than in Ref. [21]. For the range of haemoglobin variation from 80 to 170 g/L that corresponds to the measurement range of Masimo monitors, we obtained the 95% confidence interval 62.3 g/L with 8 factors and 65.5 g/L with three factors R_1, R_2, R_4, using our experimental multiwave system. The root-mean-square deviation amounted to 12.3 g/L in the first case and 14.7 g/L in the second case. The group with the haemoglobin variation range from 80 to 170 g/L was selected from the initial group and included 64 patients.

Since our system of multiwave noninvasive assessment of haemoglobin concentration is aimed at the population screening, the achieved accuracy can be considered acceptable for revealing the persons with potential pathologies. With such measurement error it is possible to reduce the probability of missing the disease by choosing appropriately the diagnostic thresholds, by increasing the measurement time in the case of weak peripheral pulsation signal, and by taking the risk factors and clinical symptoms into account. For example, in the technique for medical application one can set the thresholds of directing the patient to the laboratory examination corresponding to the haemoglobin at the level of the norm limits. However, all this requires further studies aimed at getting the a priori distributions of the haemoglobin concentrations in the population, both for healthy people and those with pathologies affecting the blood haemoglobin concentration.

5 Conclusion

The studies have shown that for assessment of blood haemoglobin concentration with the accuracy comparable with that of commercially produced monitors Rad-57 and Raical-7 (Masimo) it is sufficient to use four wavelengths of probe radiation $\lambda_1 = 658$ nm, $\lambda_2 = 776$ nm, $\lambda_4 = 974$ nm, and $\lambda_5 = 1348$ nm. In this case for the haemoglobin concentration range from 80 to 170 g/L the root-mean-square deviation that characterises the accuracy and equals to 14.7 g/L and the 95% confidence interval equal to 65.5 g/L are none the worse than the values presented in literature. To our opinion, such factor as the quality of the recorded signal affects the accuracy much stronger than the reduction of the probe wavelengths number. Further improvement of the accuracy of the assessment of blood haemoglobin concentration may be achieved by developing high-efficiency signal processing algorithms, which could, e.g., adaptively change the measurement time and their own parameters depending on the signal-to-noise ration and the character of noise.

Thus, the exclusion of $\lambda_3 = 839$ nm practically does not worsen the results and allows the simplification of technical implementation, which, in turn, reduces the cost of the system for the noninvasive haemoglobin concentration assessment.

Destruction of a spherical polystyrene microparticle in pulsed ultraviolet beam for micromanipulation purpose

Roman V. Skidanov, and Vadim S. Vasiliev*
Department of Technical Cybernetics, Samara State Aerospace University, 151 Molodogvardeyskaya Str., Samara 443086, Russia

* **e-mail:** vadimka.vasilev.93@mail.ru

Abstract. The modelling of heating a spherical polystyrene microparticle by the laser beam having the wavelength 355 nm and varying spot size is described. The simulation results are presented for two different values of the beam spot radius. Nature experiments are reported aimed at measuring the velocity of a particle with the radius 5μm accelerated by microexplosion of the neighbouring particle. © 2016 Journal of Biomedical Photonics & Engineering.

Keywords: microexplosion, ultraviolet light beam, polystyrene microspheres, microparticle velocity.

Paper #2995 received 2016.03.11 revised manuscript received 2016.03.24; accepted for publication 2016.03.24; published online 2016.03.31. doi: 10.18287/JBPE16.02.010306

References

1. P. Zemánek, A. Jonáš, L. Šrámek, and M. Liška, "Optical trapping of nanoparticles and microparticles by a Gaussian standing wave," Opt. Lett. 24(21), 1448 (1999).
2. A. K. De, D. Roy, A. Dutta, and D. Goswami, "Stable optical trapping of latex nanoparticles with ultrashort pulsed illumination," Applied Optics 48(31), G33 (2009).
3. L. Bosanac, T. Aabo, P. M. Bendix, and L.B. Oddershede, "Efficient Optical Trapping and Visualization of Silver Nanoparticles," Nano Letters 8(5), 1486-1491 (2008).
4. G. Thalhammer, R. Steiger, M. Meinschad, M. Hill, S. Bernet, and M. Ritsch-Marte, "Combined acoustic and optical trapping," Biomed. Opt. Express 2(10), 2859 (2011).
5. R. V. Skidanov, A. A. Morozov, and A. P. Porfirev, "Composite light beam and microexplosion for optical micromanipulation," Kompyuternaya optika 36(3), 371-376 (2012) [in Russian].

1 Introduction

At present, all studies on manipulation are progressing towards the reduction of the moved object size. [1-3]. A variety of methods for manipulating microparticles using optical traps of different types exists. However, it is desirable to have a method for moving relatively large microscopic objects (larger than 30 μm). Such objects most frequently observed in biological studies (spores, tissue microsamples, large cells). In this case, it is desirable to prevent the light incidence on the microscopic object. Mechanical manipulations can be implemented using mechanical tweezers; however, it can damage the moved object.

The characteristic size of the objects moved by a common optical trap varies from parts of a micrometre to nearly ten micrometres. With the increase of the object size, an essential increase of the light beam power is necessary. Due to the absorption of the light beam energy, the maximal size exists for the microparticle that can be moved at the expense of optical capture forces. The exact value of this size depends on many parameters, e.g., the absorption coefficient of the microscopic object, the properties of the liquid, the surface shape of the object, etc. Approximate estimation of this size yields about 30 μm for spherical transparent microscopic objects. It is worth noting that the object with the size close to this limit value experiences extreme thermal load. Even worse is the situation for manipulating with non-transparent objects by means of light traps. In this case, the limiting size is reduced by 1.5-2 times. A rather sophisticated method of combined trapping exists for such microscopic objects [4], e.g., using light and ultrasound. In Ref. [5] a simpler method of driving such

microobjects is described, basing on microexplosions of polystyrene microparticles in the ultraviolet laser beam with the wavelength 355 nm.

Using this method it is also possible to move sufficiently large microobjects (including the biological ones) without loss or partial destruction of the manipulated object. Using the microexplosion one can implement the displacement of the adjacent object with definite direction and distance.

The subject of the present study are the motion parameters of microobjects driven by the explosion of a polystyrene microparticle.

The goal of this works was to calculate, simulate and experimentally verify the parameters at which the spherical polystyrene particle explodes in the pulsed ultraviolet laser beam.

In correspondence with the goal, the following problems were formulated:

• development of the method for calculating the parameters, at which the microparticle explosion occurs, such as the microparticle temperature and the minimal power, providing the explosion;

• conduction of natural experiment on the microparticle explosion and qualitative comparison of the results with those obtained by simulation;

• calculation of particle dispersion velocity for different focusing objectives (20×, 40×, 100×).

2 Mathematical model describing the heating of a polystyrene particle

The heating of a polystyrene particle under the effect of pulsed ultraviolet laser radiation can be described by the heat conduction equation with the boundary conditions:

$$\begin{cases} \dfrac{\partial u}{\partial t} - a^2 \Delta u = f(r,t); \\ u\big|_{t=0} = T_0; \\ u\big|_{r=R} = T_0, \end{cases} \qquad (1)$$

We additionally consider the equation for the initial layer r_0 having the form

$$u_1 = \frac{P}{cm}\frac{(r_1 - r_0)}{r_1} + u\big|_{t=0}.$$

For the convenience of numerical solution let us consider the two-dimensional case with the nodes of the coordinate grid (r_i, t_k). After the discretisation of each component in Eq. (1), transformation to cylindrical coordinates and taking the spherical symmetry of the problem into account (all heat is accumulated in the centre and propagates in all directions uniformly) we arrive at the following formula:

$$\frac{u_i^{k+1} - u_i^k}{h_t} - a^2 \left(\frac{u_{i+1}^{k+1} - 2u_i^{k+1} + u_{i-1}^{k+1}}{h_r^2} + \frac{2}{r_i}\frac{u_{i+1}^{k+1} - u_i^{k+1}}{h_r} \right) = \frac{P}{cm}, \qquad (2)$$

where P is the power of laser radiation, c is the specific heat capacity of the polystyrene particle.

3 Results of modelling

We present the results of the modelling carried out with different parameters of laser impact. The results of the modelling are presented in Figs. 1 and 2.

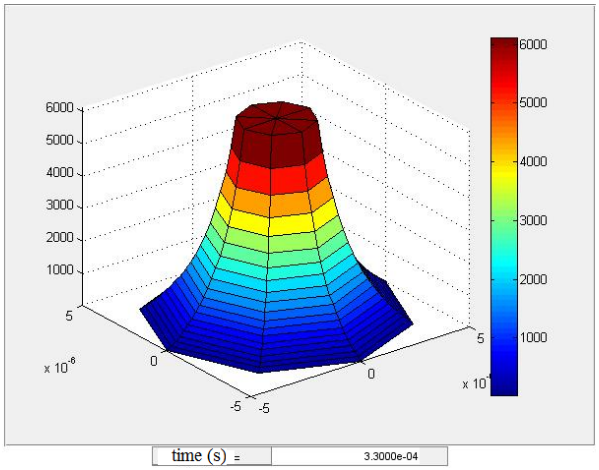


Fig. 1 Modelling of the polystyrene particle heating process with the parameters used in the experiment.

Figure 1 shows the results of modelling with the following parameters: the laser radiation power 15.4 mW, the pulse repetition rate 3000 Hz, which corresponds to the period of $0.33 \cdot 10^{-3}$ s. The diameter of the polystyrene particle was 5 μm and the laser beam spot diameter at the particle surface was 1.5μm. These parameters correspond to the experimental ones. One can see that in this case the maximal temperature amounts to 6114 K. This is much higher than the temperature of polystyrene destruction. This model is correct only below a certain temperature, because the base material of the microobject becomes modified. However, the model demonstrates that such critical parameters are achieved in a very short time, i.e., one pulse with the duration 5 ns is sufficient for complete explosive destruction of the microparticle, which will be experimentally confirmed below.

Let us see what happens if the diameter of the beam spot at the particle surface increases to 3 μm, which corresponds to using the focusing objective 40×. This situation is illustrated in Fig. 2. All other parameters are the same as in Fig. 1.

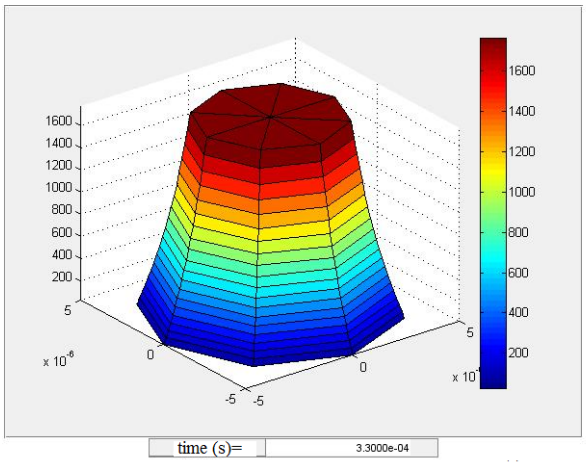


Fig. 2 Modelling of the polystyrene particle heating process with the parameters used in the experiment and the laser spot diameter of the particle surface equal to 3 μm.

Now the maximal value of the temperature appears to be 1761 K. As seen from the simulation results, during the pulse with the energy about 5.4 μJ the polystyrene microparticles is also heated to significant temperatures that exceed the temperature of polystyrene destruction. Since the model allows only the estimation of the heating parameters below the temperature of polystyrene destruction, the quantitative estimation of the microexplosion parameters requires natural experimental study.

4 Experiment

The schematic diagram of the experimental setup is presented in Fig 3. The setup incorporates the ultraviolet (UV) laser DTL-375 with the wavelength 355 nm and the maximal mean power 40 mW (the maximal pulse energy 5.6 μJ, the pulse duration 10^{-9} s, the pulse repetition rate 3000 Hz), the rotary mirrors M_1, M_2, M_3; the illumination lamp I, the focusing microscope objective L_1 (20×, 40×, 90×); the imaging microscope objective L_2 (16×); the CCD camera and the substrate with microobjects V. In the experiment, we used the DDC camera FastVideo 500 E with the resolution 640×480.

The substrate was made of silica glass. This material does not absorb light in the UV range, thus excluding the microexplosion due to the heating and melting of the glass surface. Below we present the experimental results on the microparticle explosion far from the surface of the silica substrate.

Using multiple recorded frames, we calculated the mean values of the velocity of the polystyrene particles pushed away by the explosion of the neighbouring polystyrene particle with the diameter 5 μm.

The calculations were carried out with 3 different focusing microscope objectives (20×, 40×, 100×) to determine the optimal parameters of focusing.

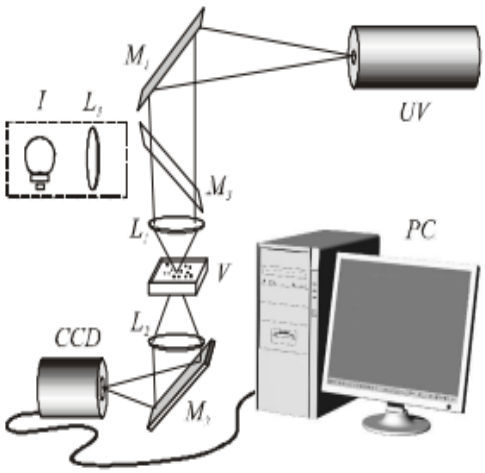


Fig. 3 Optical scheme of the experimental setup for investigating the explosion of polystyrene microparticles.

For the focusing objective 20× the beam diameter amounted to 8 μm, and the diameter of the spot on the particle was 4-5 μm. The mean velocity of spreading polystyrene particles amounted to 15.53 mm/s.

For the focusing objective 40× the beam diameter amounted to 4 μm, and the diameter of the spot on the particle was 2-3 μm. The mean velocity of spreading polystyrene particles amounted to 10.53 mm/s.

When using the focusing objective 100× the beam diameter amounted to 1.5 μm, and the diameter of the spot on the particle was 1 μm. The mean velocity of spreading polystyrene particles amounted to 9.61 mm/s. As seen from the results, the increase of the objective focal power did not increase the energetics of microparticle motion. This fact is probably due to large losses of light in the objectives with high magnification.

5 Conclusion

In the course of performing the present work, the following results were obtained:

- The model of heating a spherical polystyrene microparticle with the laser beam focused at the microparticle centre was developed. The results of modelling at different parameters were obtained.

- The velocities of particles spreading by the microexplosion were experimentally determined using different focusing objectives. For the objectives 20×, 40×, and 100× the mean velocity amounted to 15.3, 10.53, and 9.61 mm/s. The decrease of the particle velocity is obviously due to the loss of light in microscope objectives, which is essentially higher in the objectives with higher magnification.

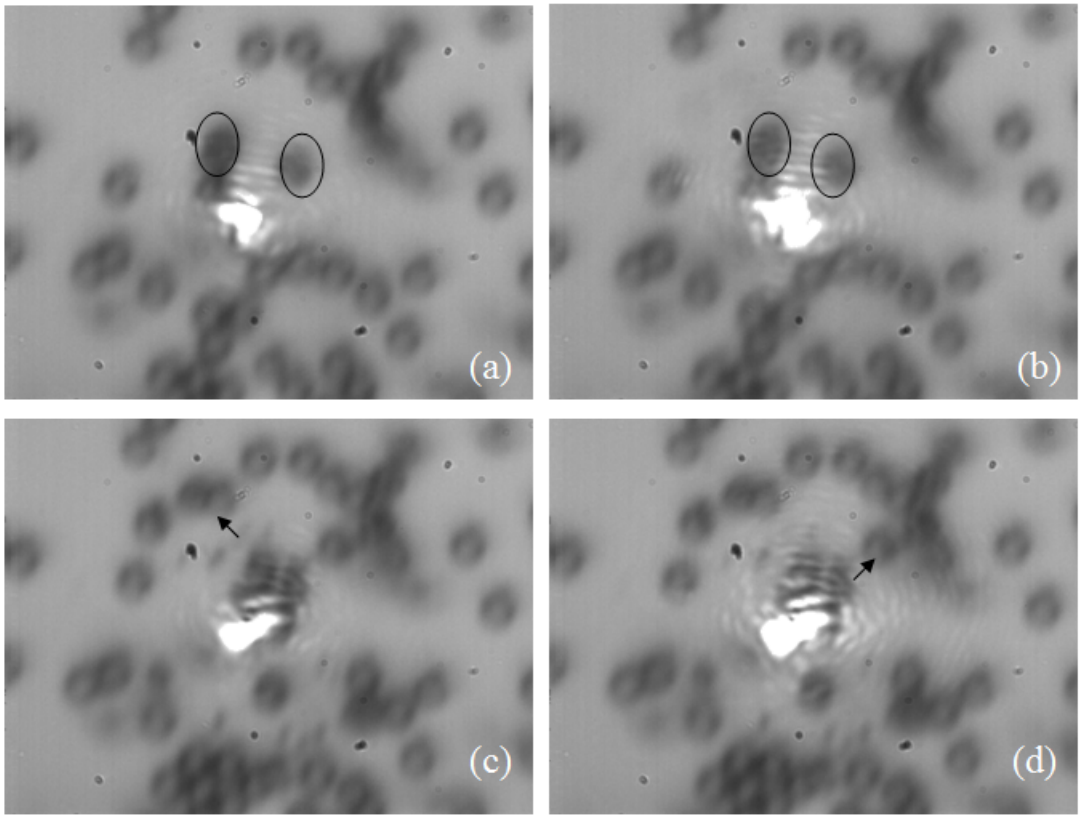


Fig. 4 Displacement of polystyrene microparticles due to the central particle explosion, recorded with the time interval 0.525 ms, the image scale being 1 μm in 1 mm.

Craquelure structure of protein film modification under the laser radiation of different spectral range action

Alexander N. Malov, Anna V. Neupokoeva*, and Evgeniya M. Kudryashova
Department of Medical and Biological physics, Irkutsk State Medical University, 1 Krasnogo Vosstaniya Str., Irkutsk 664009, Russia

* **e-mail:** annett_2005@inbox.ru

Abstract. A craquelure structure of protein film as indicator of macromolecule state is discussing. Craquelure is a network of fine cracks or crackles on the surface of a painting, caused chiefly by shrinkage of paint film or varnish. The actions of laser radiation in the red and green spectral region on the protein film craquelure structure by the example of albumin are considering. It is experimentally shown that after drying the protein layer a craquelure pattern (variety of cracks in the layer) is formed with the parameters strongly modified by the laser action and depending on the wavelength of radiation and the time (energy density) of exposure. © 2016 Journal of Biomedical Photonics & Engineering.

Keywords: craquelure, crack, albumin, film, image processing, structure monitoring, laser biostimulation.

Paper #2989 received 2016.02.29 revised manuscript received 2016.03.23; accepted for publication 2016.03.23; published online 2016.03.31. doi: 10.18287/JBPE16.02.010307

References

1. N. Y. Ilyasova, A. V. Kupriyanov, and A. G. Khramov, Information technologies of image analysis in the problems of medical diagnostics, A. S. Bugayev (ed.), Radio i svyaz, Moscow (2012) [in Russian].
2. E. G. Rapis, "Self-assembly of cluster protein films (allotropic nonequilibrium noncrystalline modification) during the process or their condensation," Technical Physics 45(1), 121-131 (2000).
3. E. Rapi, "Properties and symmetry of the solid cluster phase of protein," Technical Physics 46(10), 1307–1313 (2001).
4. E. Rapis, "A change in the physical state of a nonequilibrium blood plasma protein film in patients with carcinoma," Technical Physics 47(4), 510–512 (2002).
5. Y. Y. Tarasevich, "The models and mechanisms of the dehydration self-organization of biological fluids," Physics-Uspekhi 47(7), 717–728 (2004).
6. A. N. Malov, E. S. Musatova, A. U. Setejkin, and S. V. Zinoviev, "Laser nanoclasterization processes simulation," Modern Problems of Nanopharmacology, The 8th Russia and China Pharmaceutical Forum, 14- 17 September 2011, Blagoveshchensk, 66 – 67 (2011).
7. A. N. Malov, E. S. Musatova, and A. Y. Seteikin, "Crystallographic recording of the results of laser-induced nanoclusterization of bioorganic fluids," V-th Troitsk Conference "Medical Physics and Innovations in Medicine", Book of Proceedings, vol. 2, OOO "TROVANT", Troitsk, Moscow Region, 80 – 82 (2012) [in Russian].
8. A. N. Malov, E. S. Musatova, and A. Y. Seteikin, "Study of specific features of nucleation in the planar crystallisation of bioorganic solutions on a solid substrate," Vestnik Amurskogo gosudarstvennogo universiteta 57, 39 – 44 (2012) [in Russian].
9. A. N. Malov, A. Y. Seteikin, A. V. Neupokoeva, E. S. Musatova, I. E. Golub, L. V. Sorokina, V. S. Fetschenko, and A. A. Vaichas, "The laser radiation action on the biological objects," Optik 124, 6034-6041 (2013).
10. S. Bucklow, "The Description and Classification of Craquelure," Studies in Conservation 44(4), 233-244 (1999).
11. W. V. Moreau, Microdevices. Physics and Fabrication Technologies, Plenum Press, New York (1988).

1 Introduction

One of the main paradigms of medicine is that the pathologic organism status is reflected in the fluids that wash the cells of the body [1]. That is why in any patient the general analysis of blood and urine is performed first. However, solely the chemical analysis does not provide sufficient information, since it is unable to reveal the conformation modifications of the biological protein macromolecules. Besides, the conformation modifications of the protein molecules can manifest themselves before the chemical changes of the blood (urine) composition, or the clinical symptoms of the disease. Therefore, the early diagnostics is often possible using crystallograms.

In recent time the methods of analysing the crystallograms of biological fluids, produced by dehydration self-organisation of the protein solutions and other substances in the process of drying the solution on a solid substrate are in progress [1- 5]. It is found that the patterns that appear in this case correlate well with the patient's health [1, 4]. It was also found that the method of film crystallograms is capable of detecting the result of the laser radiation action on a biological fluid [6- 9], namely, the size reduction of the structure elements consisting of macromolecules is recorded (the phenomenon of laser-induced nanoclusterization).

The known studies in this field, as a rule, considered the dehydration of the fluid droplets on the substrate, when the formation of the crystal structure can be affected by both the change of the droplet area and the change of the wetting contact angle [5]. The difficulties can be avoided using the planar layers of protein, when the geometry of the films minimally changes in the drying process. By the end of drying the protein layer becomes covered with cracks forming a specific pattern referred to as craquelure pattern. The craquelure pattern (in French called *craquelure*) is formed by cracks of paint or varnish layer covering an oil-painted picture, which is known in art for a long time [10]. The cracks, i.e., the integrity defects of the layer of paint, varnish, or ground of a picture, possess various characters and pattern and directly depend upon the fluid composition and the cause of their origin. The craquelure effect also is used in manicure technologies.

In the present paper we consider the laser radiation action on the craquelure pattern of a protein film by the example of albumin. Possible applications of this effect may be related both to the control of the forming patterns aimed at the facilitation of decoding the resulting craquelure patterns and to the determination of the energy doses when exposing, e.g., medication solutions with the aim to activate them (similar to the analgesic activation under the intravenous irradiation of blood [9], which, in turn, allows the reduction of the narcosis amount).

2 Crack formation in polymer layers

In the process of dehydration (drying) of a biological fluid in the form of a film poured onto a solid (usually glass) substrate a number of processes simultaneously occur. They are the evaporation of the solvent (water), the diffusion of the solution components over the film, the sedimentation of molecules and their associates onto the substrate, the modification of molecular conformations, and the swelling-induced variation of the film thickness [1, 5, 10, 11]. As a whole, the drying film can be considered as possessing a layered structure; the most massive macromolecules and their associates are the first to be attached to the substrate as having the minimal velocity of thermal motion. Then they play the role of nucleation centres in the formation of the crystallographic pattern. From the surrounding solution the growth of crystallites consisting of lighter molecules occurs reducing the concentration of the admixtures in the solvent, which in turn affects the evaporation rate. As a result the formation of puncture-type defects can happen due to different reasons, including the excretion of dissolved gases [11].

The effect of "cracking" is based on the difference in the drying time between the underlying layer and the coating (liquid and gel-like surface layer) which is cracked. Some craquelure compositions become fully dried in several days. Such underdried composition strongly extracts water from the water-based paint or varnish material and provides a sufficiently "slippery" surface for the paint or varnish that cracks in the course of drying on it [5, 10]. The cracks can vary from the extremely fine hairline to considerable ones. The cracks, i.e., the defects of the pain, varnish, or ground layer integrity, possess different character and form different patterns directly reflecting their cause. A known from photography, besides the crack formation, the shrinkage of the surface layer (reticulation) can also occur. The action of laser radiation reduces the cluster size in a biological liquid [6- 8], which facilitates the formation of cracks, too.

3 Materials and Methods

As a model medium we used the egg protein albumin. The albumins are proteins of animal and plant tissues. They are globular proteins contained in the blood plasma and egg white, executing the transport and nutrition functions, respectively. Their content approaches 50% of the total amount of protein in the tissue. We suggest that under the action of laser radiation on blood the structure of blood proteins is changed, which is an important link in the development of the biological response to the laser impact. Therefore, if our experiments with albumin will demonstrate the change of its structure and we will be able to visualise these changes, then it will be possible to expect similar changes in the blood proteins.

As sources of laser radiation we used the semiconductor laser units with the wavelengths 530 nm and 650 nm.

After separating the egg white from yolk the white was divided into three portions. Then two portions were sequentially irradiated, the first one with the radiation having the wavelength 530 nm and the power about 80 mW (nearly 1200 mW/cm^2) during 2 minutes, and the second one with the radiation having the wavelength 650 nm and the power about 10 mW (nearly 150 mW/cm^2) during 20 minutes. Therefore, the total energy of irradiation amounted to 10 J (the energy density being nearly 150--180 J/cm^2) for each of the irradiated samples. Then all samples were poured onto glass plates and kept at room temperature until dried. After drying the protein layer acquired cracks forming the characteristic craquelure pattern.

4 Results and Discussion

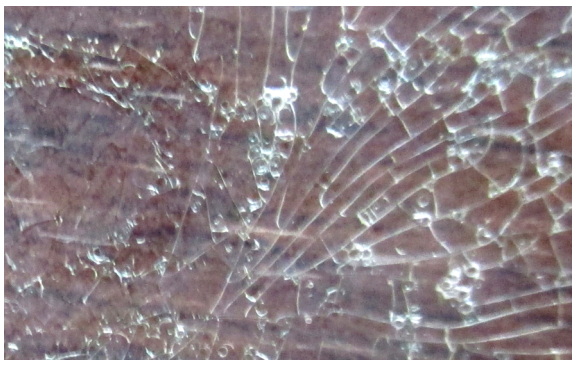
The effect of laser exposure on albumin was assessed by observing the craquelure patterns on the dried film (Fig. 1). The patterns were observed visually and using a web camera. By the naked eye it was seen that the non-exposed samples had thick and larger cracks, while the air bubbles were present in small amount. The protein structure after the laser impact is finer, the bubbles and cracks are closer to each other and smaller in size. After the irradiation with red light the number of bubbles is significantly larger, while after the irradiation with green light only the reduction of the crack size and bubble diameter occurs, their number being comparable with than in the control unexposed sample.

Using the photographs from the web camera it was calculated that the mean diameter of a bubble in the control unexposed samples was 5--6 mm and in the exposed ones 2--3 mm.

We also sought the threshold energy, i.e., the minimal energy of the laser radiation, causing the observable changes in the craquelure pattern. Figures. 2, 3 present the results of irradiating albumin with laser light with the wavelength 650 nm during different time. From the comparison of patterns obtained after different times of exposure one can see that in the control sample, after 1 and 2 minutes of exposure the patterns are similar, and the characteris-tic pattern size visible in the microscope amounts to nearly 70 μm. For the exposure time of 5 minutes it is visually seen that the structures of the pattern becomes finer. The calculations show that its diameter amounts to nearly 40 μm. For the exposure time greater than 5 minutes the structure becomes more inhomogeneous due to the appearance of small-scale elements with the size of about 20 μm.

From the presented data it follows that the changes in the pattern become observable after the exposures from 5 minutes and longer, which corresponds to the total energy of impact about 3 J (or the energy density about 50 J/cm^2).

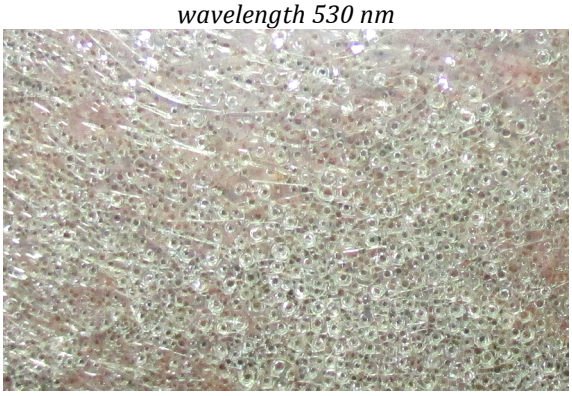
Figure 3 presents the photographs of the patterns on the albumin layer from the same series, as shown in Fig. 2. However, for clarity only the samples separated by the expose time difference of 10 minutes are left, which allows to trace the modifications by the naked eye. Thus, for the exposure time of 10 minutes the bubble size seems to decrease as compared to the control sample and continues to decrease with the increasing exposure time.



Without laser impact



After the impact of laser radiation with the wavelength 530 nm



After the impact of laser radiation with the wavelength 650 nm

Fig. 1 Typical craquelure patterns in the dry layers of albumin.

5 Conclusion

Thus, it is shown that the parameters of craquelure structure (the size of bubbles and cracks and the separations between them) are essentially reduced after the laser impact on the protein. Besides, it was found that the laser radiation with the wavelength 650 nm exerts more expressed influence on the shelling pattern of the albumin layer, and the threshold energy density is nearly 50 J/cm^2.

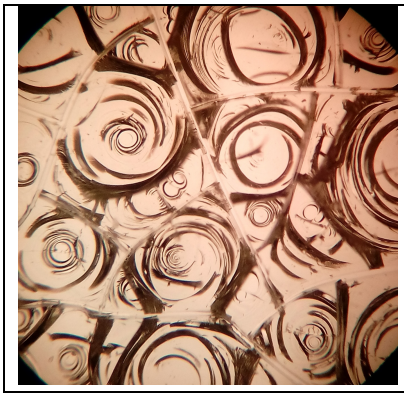
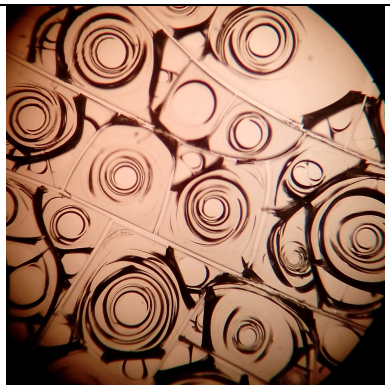
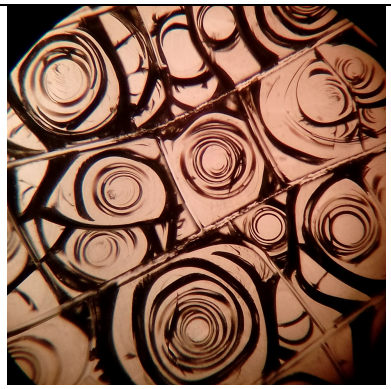
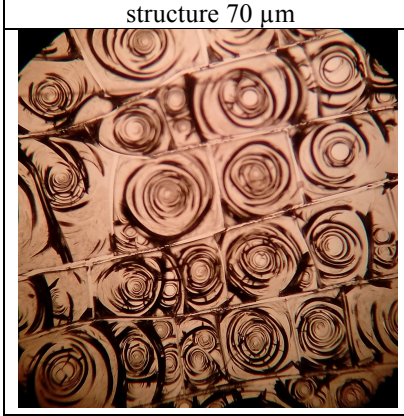
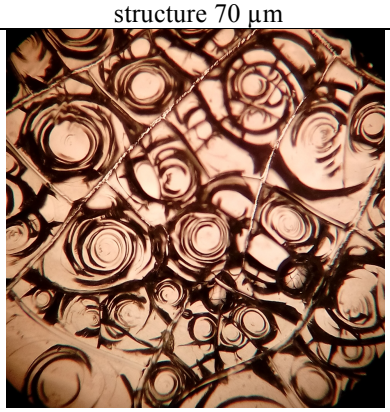
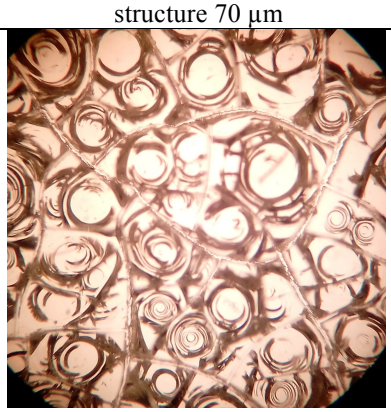
		
0 minutes; Characteristic diameter of the structure 70 μm	1 minute (9 J/cm^2); Characteristic diameter of the structure 70 μm	2 minutes (18 J/cm^2); Characteristic diameter of the structure 70 μm
		
5 minutes (45 J/cm^2); Characteristic diameter of the structure 40 μm	10 minutes (90 J/cm^2); Characteristic diameter of the structure 40 μm, but the structures of nearly 20 μm appear	20 minutes (180 J/cm^2); Characteristic diameter of the structure 20-30 μm

Fig. 2 Typical microscopic view of craquelure patterns in dry layers of albumin after different times of exposure to laser radiation with the wavelength λ=650 nm.

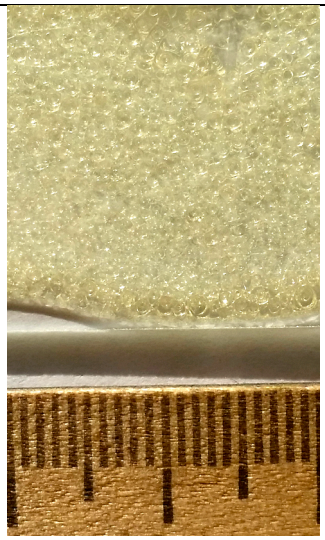
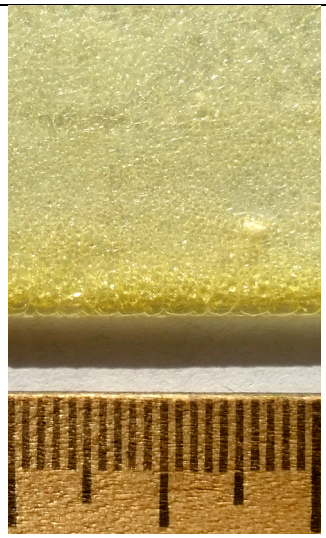
		
0 minutes; Bubble size about 1.5-2 mm	10 minutes (90 J/cm^2); Bubble size about 1 mm	20 minutes (180 J/cm^2) Bubble size smaller than 1 mm (nearly 0.6 mm)

Fig. 3 Typical view of craquelure patterns in dry layers of albumin after different times of exposure to laser radiation with λ=650 nm.